



**HAL**  
open science

## Diffusion-based culture and real-time impedance monitoring of tumor spheroids in hydrogel microwells of a suspended membrane under microfluidic conditions

Wei Wang, Yuanhui Liu, Xiaochen Huang, Feng Liang, Haoyue Luo, Zheng Mao, Jian Shi, Li Wang, Juan Peng, Yong Chen

### ► To cite this version:

Wei Wang, Yuanhui Liu, Xiaochen Huang, Feng Liang, Haoyue Luo, et al.. Diffusion-based culture and real-time impedance monitoring of tumor spheroids in hydrogel microwells of a suspended membrane under microfluidic conditions. *Talanta*, 2024, 278, pp.126473. 10.1016/j.talanta.2024.126473 . hal-04635076

**HAL Id: hal-04635076**

**<https://hal.science/hal-04635076v1>**

Submitted on 4 Jul 2024

**HAL** is a multi-disciplinary open access archive for the deposit and dissemination of scientific research documents, whether they are published or not. The documents may come from teaching and research institutions in France or abroad, or from public or private research centers.

L'archive ouverte pluridisciplinaire **HAL**, est destinée au dépôt et à la diffusion de documents scientifiques de niveau recherche, publiés ou non, émanant des établissements d'enseignement et de recherche français ou étrangers, des laboratoires publics ou privés.

# Diffusion-based culture and real-time impedance monitoring of tumor spheroids in hydrogel microwells of a suspended membrane under microfluidic conditions

Wei Wang<sup>a,1</sup>, Yuanhui Liu<sup>b,c,a,1</sup>, Xiaochen Huang<sup>a</sup>, Feng Liang<sup>a</sup>, Haoyue Luo<sup>a</sup>, Zheng Mao<sup>a</sup>, Jian Shi<sup>d</sup>, Li Wang<sup>d</sup>,

Juan Peng<sup>a\*</sup>, Yong Chen<sup>a\*</sup>

<sup>a</sup> *École Normale Supérieure-PSL Research University, Département de Chimie, Sorbonne Universités-UPMC Univ Paris 06, CNRS UMR 8640, PASTEUR, 24, rue Lhomond, 75005 Paris, France*

<sup>b</sup> *Department of Oncology, Tongji Hospital, Tongji Medical College, Huazhong University of Science and Technology, Wuhan 430030, Hubei, China*

<sup>c</sup> *Cancer Center, Tongji Hospital, Tongji Medical College, Huazhong University of Science and Technology, Wuhan, 430030, Hubei, China.*

<sup>d</sup> *MesoBioTech, 231 Rue Saint-Honoré, 75001, Paris, France*

<sup>1</sup> *These authors have equal contributions*

*E-mail: [yong.chen@ens.psl.eu](mailto:yong.chen@ens.psl.eu), [juan.wang@ens.psl.eu](mailto:juan.wang@ens.psl.eu)*

## Abstract

Tumor spheroids are widely studied for in vitro modeling of tumor growth and responses to anticancer drugs. However, current methods are mostly limited to static and perfusion-based cultures, which can be improved by more accurately mimicking pathological conditions. Here, we developed a diffusion-based dynamic culture system for tumor spheroids studies using a thin membrane of hydrogel microwells and a microfluidic device. This allows for effective exchange of nutrients and metabolites between the tumors and the culture medium flowing underneath, resulting in uniform tumor spheroids. To monitor the growth and drug response of the spheroids in real-time, we performed spectroscopic analyses of the system's impedance, demonstrating a close correlation between the tumor size and the resistance and capacitance of the system. Our results also indicate an enhanced drug effect on the tumor spheroids in the presence of a low AC electric field, suggesting a weakening mechanism of the spheroids induced by external perturbation.

Keywords: Tumor spheroids, hydrogel membrane, microfluidics, impedance

## 1. Introduction

Solid tumors with sizes of 250-750  $\mu\text{m}$  are found in cancer patients during the early stage of cancer development, while the tumor progression and metastasis is the result of a very complex relationship between different cells as well as the tumor microenvironment.[1–3] To understand the tumor growth and find new therapies, tumor spheroids are studied for in vitro modeling by using various engineering methods, including hanging drop culture, low-adhesive substrate, and microfluidic techniques.[4–17] These methods are intuitive but often limited in processing flexibility, reproducibility, or high-throughput ability. Moreover, they cannot easily recapitulate the tumor microenvironment such as blood vessels that bring nutrients into the tumor space and move away the metabolites for tumors. From a physical point of view, tumor growth can be simulated based on a convection-diffusion-reaction model. Previous studies also showed that tumor cells in a spheroid were highly heterogeneous, e.g., the cells in the core were significantly different from those of intermediate and outer layers in terms of proliferation, quiescence, necrosis, and differentiation capability, due to diffusion-limited exchange of nutrient, oxygen, and metabolites. Though this cannot be avoided, a faster clearance of metabolites outside the spheroid and a higher nutrient/oxygen concentration may improve the quality of the spheroids. This can be achieved by culturing the spheroids on one side of a porous membrane and flowing a high concentration culture medium on the other side of the membrane so that a high concentration gradient can be established without shearing the spheroids. In this regard, a microfluidic device with an increased membrane can be applied for diffusion-based culture. Previously, microfluidic techniques were mostly used to form tumor spheroids in small cavities, U-shape traps, microwells, or droplets, they were still static or perfusion-based.[6,18] Therefore, it is highly interesting to develop a diffusion-based culture method to recapitulate the early stage of tumor growth in the vicinity of a perfused blood vessel.

Another critical issue in tumor spheroid studies is the real-time monitoring of the tumor growth. This can be done by either 3D optical imaging[19] or electrical impedance spectroscopy (EIS).[20–23] Compared to the optical imaging techniques, EIS is also label-free and non-invasive, which might be low cost and more accessible for long term observation of the cell growth behaviors. The previous studies already demonstrated the reliability of EIS

analyses of single tumor spheroids by using patterned electrodes and it should be possible to analyze an array of tumor spheroids by using a microfluidic device with multiple electrodes. In both cases, the tumor spheroids are still under static or perfusion conditions and precise positioning of the spheroids with respect to the electrode array should be importance.

Despite significant advances in tumor spheroids and EIS methods, application of diffusion-based culture and real-time impedance monitoring of a large number of spheroids has remained absent from the literature. The inherent complexity in cellular microenvironment requires sophisticated microfluidic systems to support reliable exchange of nutrient and metabolites between cells and culture media. Furthermore, these systems general lack a good material compatibility for electrode integration. Here, we report a simple, robust, microfluidic technique for diffusion-based culture and real-time impedance monitoring of tumor spheroids in which a suspended membrane of hydrogel microwells is reversibly integrated into a microfluidic device. This membrane is made of polyethylene glycol diacrylate (PEGDA) and the microwells were obtained by vacuum assisted UV molding of PEGDA. PEGDA is often used for 3D cell culture due to its low surface energy and high permeability.[24–27] Moreover, the swelling effect of PEGDA can be reduced by using solvent-based processing so that the fabricated PEGDA membrane can be used as a chip insert to support the tumor growth and the integration into a microfluidic device. We show that this platform has great flexibility to generate uniform tumor spheroids and to monitor the growth behaviors of the tumors as well as their responses to anti-cancer drugs. Data obtained by optical imaging and impedance spectroscopy are compared to illustrate the relevance of the on-chip and real-time monitoring of EIS in terms of tumor grow rate. Finally, we demonstrate the possibility of enhancing the effect of anticancer drugs with a low AC electric field and discuss the potential of the present platform for both preclinical and clinical assays.

## **2. Experimental Section**

### **2.1 Fabrication of hydrogel microwell membrane**

PEGDA hydrogel membrane was fabricated by vacuum- and UV-assisted molding with a mold made of polydimethylsiloxane (PDMS) and glass slide (Fig. S1, S2). Firstly, a chromium

photomask of 12 mm outer and 8 mm inner diameters, which consists of 250  $\mu\text{m}$  diameter and 350  $\mu\text{m}$  period dot array was patterned with a micro-pattern generator ( $\mu\text{PG}$  101, Heidelberg Instruments, Germany). A 250  $\mu\text{m}$ -thick photoresist (SU-3050, MicroChem, USA) was then spin-coated on the patterned chromium layer, prebaked, and backside UV exposed, followed by a post-bake at 95°C with a hot plate. Next, it was exposed to trimethylchlorosilane (TMCS, Sigma, France) vapor and used for PDMS casting with a mixture of PDMS pre-polymer and cross-linker (RTV 615, Momentive Performance Materials) at a ratio of 10:1(w/w). After curing at 75°C for 4 h, an array of PDMS micro-posts was obtained. By stamping them against a thin layer of viscous PDMS, convex heads formed for each of the posts after curing. In parallel, a baseplate was fabricated by photomasking a 10  $\mu\text{m}$  thick SU8 on a glass slide. Finally, the PDMS layer was placed on the baseplate with the structure plane down and degassed in a desiccator for 10 min. A PEGDA solution (32 %vol DMSO; 32 %vol ethanol; 12 %vol 2-Hydroxy-2-methylpropiophenone (1173); 24 %vol PEGDA, Mw 575, all purchased from Sigma-Aldrich, France) was injected into the cavity between the PDMS layer and the baseplate. Once the cavity was completely filled with the PEGDA solution, the assembly was exposed to 18.9  $\text{mW}\cdot\text{cm}^{-2}$  UV light for 20 S. Finally, the PDMS layer was removed and the PEGDA membrane was peeled off from the glass slide, resulting in a PEGDA membrane with excellent biocompatibility, UV curability, and optical transparency (Fig. S3a-3d).[28,29]

### **2.3 Microfluidic system for automatic culture and monitoring**

A microfluidic system used in this work consists of a standard organ-chip device, a chip flow controller, and a multichannel impedance analyzer (MesoViva, France). The device is made of a plastic cover plate with female Luer connectors and a thin PDMS sealing layer and a lower plate made of a multilayer PDMS on glass slide. On both plates, microchannels were embedded and semi-open culture chambers were patterned. In addition, a thin PDMS layer with holes was bounded on the top of the lower plate for positioning the hydrogel membrane. A gold electrode was patterned on the glass slide and a platinum-coated electrode was added to the upper plate. In addition, a thin PDMS layer with circular opening was cells were seeded in the microwells and the hydrogel membrane with cells was then sandwiched by the two plates and fixed with a hand-screw clamping device. To avoid the bubble formation, the culture

medium was firstly introduced in the chambers and channels of both upper and lower plates before device assembly. Then, the hydrogel membrane with cells were carefully placed the top of the lower plate and the assemble was covered by the upper plate free of air bubbles. Next, the microfluidic device was connected to a peristaltic pump system, a culture medium reservoir and a waste container for automatic. The impedance monitoring was done with a frequency range from 5 to  $10^5$  Hz and a voltage amplitude of 0.1 V, unless specified. The raw data were analyzed using the least square method and an equivalent electric circuit.

## **2.4 Cell seeding and tumor spheroid pre-forming**

Human glioblastoma cell line U87 (Sigma-Aldrich) was prepared in Dulbecco's Modified Eagle Medium (DMEM) completed with 10% FBS and 1% penicillin/streptomycin at 37 °C with 5% CO<sub>2</sub> supplementation. Cell solutions of 0.5, 1, and 2 K/ $\mu$ l were prepared and named 20, 40, and 80K, respectively. The 40  $\mu$ l cell-containing medium was dropped to the surface of a PEGDA membrane and placed in a culture dish. After 5 min, most of the cells precipitated into the microwells of the PEGDA membrane. Then, the excess medium was extracted from the edge of the membrane. Finally, the membrane with cells was transferred into an incubator. After a few hours (6h), tumor spheroids were formed in the microwells. All PEGDA membranes were sterilization before use. The membrane was firstly soaked in 70% v/v alcohol/water for 15 min., immersed three times in PBS with a time interval of 10 min, and finally sterilized by UV irradiation for 30 min

## **2.5 SEM characterization**

Hydrogel membrane with tumor spheroids were soaked in 10% ethanol solution (in deionized water) for 1 h and then dehydrated by sequentially soaking in 20%, 30%, 40%, 50%, 70%, 90%, and 100% ethanol solution containing each for 20 min. and then dried with a vacuum pump. Then, a gold layer with a thickness of 5-10 nm was deposited by sputtering, and the samples were observed using a scanning electron microscope (SEM, Hitachi S-800, 10 kV).

## **2.6 Immunofluorescence staining and image acquisition**

Immunofluorescence staining was performed for Ki-67 and F-actin expression on day 7. Briefly, the tumor spheroids were fixed with 4 % paraformaldehyde for 20 min together with a PEGDA hydrogel membrane. The tumor spheroids and PEGDA hydrogel membrane were washed three times with PBS for five min. each time, and then the membrane was incubated in permeabilization buffer (0.2 % Triton X-100, 20  $\mu$ g/ml EDTA) for two hours. Tumor spheroids and PEGDA hydrogel were washed in washing buffer (0.3% Triton X-100, PBS) 3 times for 10 min and incubated with saturation buffer for 1 h at room temperature. Then dilute the primary antibody (Ki-67) in wash buffer and incubate overnight at 4°C. PEGDA hydrogel membrane and cells were washed 3 times with wash buffer for 10 min. each time, and secondary antibodies (anti-Rabbit 555) were briefly released in a washing buffer solution, and incubated at room temperature for two hours. Then, 300 ng/mL 4'-6-diamidino-2-phenylindole (DAPI) (1:50 dilution, Sigma) and F-actin (1:50 dilution, Sigma) was used to label nuclei for 15 min, followed by washing with PBS. Samples were washed 3 times with PBS and imaged using a confocal laser scanning microscope

## **2.7 Anti-drug response and live/dead assay**

DOX was mixed in D.I. water to prepare a solution of 2 mg/ml DOX concentration and then stored at 4 °C. Before use, the solution was further diluted in DMEM to obtain the desired DOX concentration. After the tumor spheroid formation, they were stabilized in an FBS-free medium for 15 h, and then in a DOX-containing medium for 40 h in an incubator at 37°C and 5% CO<sub>2</sub>. Afterward, impedance spectra were recorded automatically.

Live and dead cell staining was performed with PBS solutions containing 2  $\mu$ M Calcein AM and 3  $\mu$ M Propidium iodide (PI), respectively. After incubation for 30 min at 37°C and 5% CO<sub>2</sub>, the solution was washed off twice with fresh PBS. The cells were then fixed in 4% paraformaldehyde solution for 15 min and permeabilized in 0.5% Triton X-100 for 20 min at room temperature. Then, 300 ng/ml DAPI (1:100 dilutions, Sigma) was used to label nuclei for 15 min, followed by washing with PBS. Finally, the stained cell spheroids were transferred to glass slides for fluorescence observation with an inverted light microscope (Zeiss, Axiovert 200) equipped with a digital CCD camera (Evolution QEI). Viability was calculated by

dividing the number of viable cells by the number of total cells. All data were analyzed by Image J software.

## **2.8 Application of biochemical and biophysical stimuli**

Before stimulation, all tumor spheroids samples were stabilized in a calcium ion-free medium for 4 h. Three groups of assays were evaluated: (1) electrical stimulation alone (0.2V, AC 500Hz), (2) incubation with EDTA but without electrical stimulation, and (3) incubation with EDTA in the presence of electrical stimulation. The upper and lower chambers of the chip were kept in a medium containing the same concentration of EDTA during the experiment. To observe more clearly the effect of EDTA, the 2 mM EDTA medium was replaced by a 4 mM EDTA medium after 30 min incubation. The electrical stimulation was performed for 10 sec. each 5 min.

## **3. Results and discussion**

### **3.1 Characteristics of the hydrogel microwell membrane**

The fabricated PDMS micro-posts showed well-defined convex heads, resulting in a PEGDA membrane with microwells with concave bottom of 5  $\mu\text{m}$  smallest thickness (Fig. 1). In total, 473 microwells were obtained in an area of 8 mm diameter with a ring. To reduce the swelling effect, a DMSO/ethanol binary solvent was used for the preparation of the PEGDA solution. Our results showed that the fabricated hydrogel membranes were plate and could be manipulated with a tweezer repeatedly (Fig. S3b). This solvent-based PEGDA (S-hydrogel) showed also better wetting stability (Fig. S3c) and better optical transparency (Fig. S3d), compared to the water-based PEGDA (W-hydrogel). When submerged in water, W-hydrogel was shrunken due to the counter ions in the gel. When submerged in water, PBS, or culture medium, the S-hydrogel was stable and insensitive to the pH value of the solution, due to its high degree of crosslinking.[30,31] The fabricated PEGDA membrane is highly permeable to nutrient and metabolites not only due to the high porosity of the hydrogel network but also due to its limited thickness.[24–27] In fact, the smallest bottom layer thickness of the microwells is only a few micrometers, suggesting a comparable nutrient concentration in the microwells than that of the culture medium underneath the membrane. Since the culture medium was

flowing, a high concentration gradient could be maintained for the tumor growth. Glucose has a molecular weight of 180 Da and a size of about 1 nm so it can easily diffuse across the PEGDA membrane. As control, we also performed static culture with the same type of hydrogel membrane. Now, the hydrogel membrane was attached on the bottom of a chamber of 24 well plate. and a cell containing culture medium was supplied for cell seeding. For comparison, only 200  $\mu$ L per well was used and renewed each two days. Our results showed a comparable growth rate in both case, suggesting the relevance of microchannel based dynamic diffusion culture chip (Fig. S4). Clearly, the hydrogel membrane based diffusion culture is also preferable to the conventional perfusion culture since the cells are not subjected to any shear stress. In terms of growth rate, the diffusion-based culture is less efficient than perfusion and static culture with over supplied nutrient but it is still significantly higher than the in vivo solid tumors. A relevant growth rate control might be useful for in vitro studies

### **3.2 Microfluidic system for automatic culture and impedance monitoring**

Fig.2 shows a schematic diagram and a photograph of the microfluidic system developed in this work. Here, the hydrogel microwell membrane separated the culture chamber is two parts, and the exchange of nutrients and metabolites between tumor cells and the lower chamber stream was diffusion-based due to the small thickness of the bottom of hydrogel microwells. The chip flow controller was made of two peristaltic pumps, two solenoid pinch valves, and electronic accessories. The multichannel impedance analyzer was composed of an analyzer of Analog Discovery 2 (Diligent, France) and a multiplexer. Python script was prepared to control automatically the culture and data recordings. For simplicity, the culture medium in the upper chamber remained static, while the medium in the lower chamber was renewed once per hour, each time lasting for 10 min. at a rate of 60  $\mu$ l/min, considering the glucose and oxygen consumption of the spheroids (SI method 1).

### **3.3 Growth of the tumor spheroids**

U87 cells were used for the system validation. Before its usage, the PEGDA membrane was stored in PBS to avoid dehydration-induced deformation. After seeding, cells formed aggregates in the PEGDA microwells and then tumor spheroids one day after seeding before being transferred into the microfluidic device for diffusion-based culture.[16] As a result, the

cells continuously grew for 12 days with a typical growth behavior of tumor spheroids (Fig. 3a). Statistically, the cell number in microwells was slightly smaller than the expected value due to the removal of the excess medium at beginning which contained a small number of cells (Fig. 3b). Depending on the number of seeding cells, the sizes of the spheroids were different but the formation ratio of the spheroids in the microwell in all cases was 100% and no cell was found outside of the microwell during the whole growth period. Typically, a growth plateau appeared after a fast-growing period (Fig. 3c) and the increase in cell number as a function of incubation time was cell-seeding dependent (Fig. 3d).

Phenomenologically, the growth behavior of tumor cells can be described by Gompertzian function,[4]

$$V(t) = V_{max} \exp \left\{ -\ln \left( \frac{V_{max}}{V_{init}} \right) \exp(-\alpha t) \right\} \quad (1)$$

where  $V$  is the spheroid volume,  $t$  is the incubation time,  $\alpha$  is the specific growth rate, and  $V_{init}$  and  $V_{max}$  are the initial and plateau volume of the spheroid, respectively. This model predicts an exponential growth phase and a growth plateau due to the increasing number of quiescent cells and the accumulation of necrotic cells in the core of the spheroid. As can be seen in Fig. 3e, our experimental data suggested that the tumor growth was Gompertzian-like but not logistical-like and different sets of fitting parameters could be obtained for different cell seeding numbers. Cell seeding and aggregation with more cells resulted in even larger tumor spheroids (Fig. S5a).

The size uniformity and the circularity of the tumor spheroids obtained were both excellent (Fig. 3f-3g, Fig. S5b). Here, 6 zones were randomly selected to measure the diameter of the spheroids, while the circularity of the spheroids was determined by definition, i.e.,  $S = 4\pi A/P^2$ ,  $A$  is the area projected by the spheroid, and  $P$  is the circumference of the circle. For a perfect spheroid,  $P = 2\pi r$  and  $S = 1$ . After dehydration, the spheroids were observed by SEM, showing a spherical and compact form of the spheroids with distinct individual cells (Fig. 4a,4b). From the SEM images, the uniformity and the sphericity of the tumor spheroids were also confirmed. In addition, the spheroid-associated extracellular matrix was also visible.

Generally speaking, tumor spheroids in hydrogel microwells are compact due to non-adherent walls and E-cadherin mediated cell-cell interaction.[32] During tumor growth, the

spheroid forms different layers, i.e., a proliferative outer layer, a quiescent layer, a hypoxic layer, and a necrotic core, due to limited inward diffusion of oxygen and nutrients and limited outward diffusion of carbon dioxide and waste in the spheroid.[4–7,33] Our results of Ki67 staining showed a low expression level of the cells in the core of spheroids after culture for 7 days (Fig.4c). Here, Ki-67 was a marker associated with the proliferation capability of the cells, suggesting that the cells in the center part of the spheroids were in a necrosis state. Moreover, the actin expression of the cells in the intermediate layers was homogeneous, while that of the outer layers showed remarkable nonhomogeneous distribution due to the differences in the proliferation activity of the cells.

The cell viability of the tumor spheroids was evaluated by dead/live assays (Fig. 4d), showing that the cells in the tumor spheroids have a high survival rate due to the relatively small size of the spheroids. This could also be attributed to more efficient diffusion across the membrane due to dynamic culture under microfluidic conditions, which renew constantly the medium and ensure a high concentration gradient of nutrients and metabolites.

### 3.4 Impedance spectroscopy

The impedance of a membrane-based system is mostly sensitive to the current leakage across the membrane, while is also sensitive to the dielectric property of the membrane and species on the membrane. This is particularly relevant to access the integrity of the membrane and the species wherein. Theoretically, the impedance of a membrane system can be calculated by considering the resistance and the capacitance of all involved components, including hydrogel microwells, growing tumor spheres, electrolytes, and the specificity of electrodes. Depending on their arrangement, an equivalent electric circuit can be worked out for more detailed calculation.

The impedance spectra were analyzed using an equivalent electric circuit from which both resistance and capacitance of the spheroid,  $R_{sph}$  and  $C_{sph}$ , could be deduced (Fig. 5a, SI Method 2). The other parameters of the circuit, including  $R_{ext}$ , the resistance of the free area of microwell,  $R_{m1}$  ( $R_{m2}$ ) and  $C_{m1}$  ( $C_{m2}$ ), the resistance and capacitance of the thicker (thinner) portion of the membrane,  $R_{bulk1}$  ( $R_{bulk2}$ ), the resistance of the culture medium in the upper (lower) chamber, and  $CPE_1$  ( $CPE_2$ ), the constant phase element of the top (bottom)

electrode, were also considered. For simplicity, the contribution of  $C_{m1}$  ( $R_{m2}$ ) and  $C_{m2}$  could be neglected due to the large (small) thickness and the small area of the bottom layer of the membrane. Then, the following transfer function could be used[34]

$$Z = Z_{CPE} + R_{bulk} + Z_{sph} \quad (2)$$

with

$$Z_{CPE} = \frac{1}{A(j*2\pi f)^n} \quad (3)$$

and

$$Z_{sph} = \frac{R_{sum}}{1+j*2\pi f*C_{sph}*R_{sum}} \quad (4)$$

where  $Z_{CPE}$  is the sum of two constant phase elements of the electrodes,  $R_{sum}$  is obtained from  $R_{m1}$ ,  $R_{sph}$  and  $R_{ext}$ ,  $f$  is the frequency, and  $A$  and  $n$  are two parameters of the  $Z_{CPE}$ . Fig. 5b illustrates the contribution of each involved component with a set of fitting parameters. Clearly,  $Z_{CPE}$  is reversely proportional to frequency in a log-log graph so that the low-frequency region of the spectrum is dominated by  $Z_{CPE}$  while the high-frequency region of the spectrum is determined by  $R_{bulk}$ . In the mid-frequency region, the spectrum is more sensitively dependent on the membrane properties and the presence of tumor spheroids. Roughly speaking, the mid-frequency impedance increases with  $R_{sum}$  and redshifts with the increase of  $R_{sum}$  and  $C_{sph}$ .

Experimentally, we first analyzed the impedance data with 100  $\mu\text{m}$  and 250  $\mu\text{m}$  thick flat PEGDA membranes (Fig. S6a). As expected, the resistance increased quasi-linearly with the thickness of the membrane (Table S1, Fig. S6b), giving a material resistivity of 1.79  $\Omega \cdot \text{m}$ . Then, the resistance of a thickness  $x$  is calculated,  $R_x = xR_{250}/250$ , where  $R_{250}$  is the resistance of 250  $\mu\text{m}$  thick layer, from which the effective thickness of the bottom layer can be deduced from,

$$x = \frac{250*S_w}{R_{250} - (1-S_w)*R_{250w}} \quad (5)$$

where  $S_w$  and  $R_{250w}$  are the total area of the microwells and the resistance of the membrane, respectively. A bottom thickness of 76  $\mu\text{m}$  was obtained, which is small enough for molecule diffusion but larger than that estimated from the SEM image, due probably to the non-flatness of the bottom layer.

Fig. 5c shows typical impedance spectra of the spheroids before and after culture for 12 days. Impedance spectra differences are subtle on the log-log plot, but significant variations in spheroid deduced resistance and capacitance over time are evident in Fig. 5d and 5e. The real part of impedance at 5 Hz shows varying behaviors over time with different cell seeding numbers (Fig. S7). Peaks appear earlier with larger cell seeding numbers, preceding the impedance plateau. Spheroids from 20K cells stabilize at day 10 (max capacitance  $\approx 37 \mu\text{F}$ ), while those from 40K and 80K cells stabilize at day 8 and day 6, respectively.

Considering the similar behavior of the size, resistance, and capacitance changes, one can suggest that the change in resistance and capacitance of the system was due to the size increase of the tumor spheroids. Thus, impedance monitoring is useful for the determination of the growth behavior of the tumor spheroid. Moreover, the resistance and capacitance of single spheroids ( $r_{sph}$  and  $c_{sph}$ ) can be deduced by considering the total number of spheroids on the membrane ( $N \sim 500$ ). Neglecting the contribution of the hydrogel,  $r_{sph} = NR_{sph}$ , and  $c_{sph} = C_{sph}/N$ , which give rise to a spheroid resistance in the range of 75 k $\Omega$  to 450 k $\Omega$ , and a spheroid resistance in the range of 10 nF to 85 nF. Based on the spectroscopic analyses, however, one cannot assess neither the shape nor the size distribution of the spheroids. In fact, our system with only one pair of electrodes was used for general assessment of the tumor growth, which could be fairly correlated to the results of optical and SEM techniques. Nevertheless, the change in resistance and capacitance of the system can reflect the change in size of the spheroids in the microwells, which might be easy to use for real-time monitoring.

To understand the size-dependence of the impedance, a simple calculation was carried out (SI method 2, method 3, and Fig. S8). Roughly speaking, the increase in spheroid size leads to an increase in both resistance and capacitance of the system due to the increase of cell number and the decrease of the free well space. Here, the distribution of electric field lines was simulated using a 2D model and Comsol software. For comparison, two types of microwell profiles were considered, showing that the electric field strength is higher in the free space of the microwell than in other parts (spheroid and thick hydrogel part). When the spheroid is comparable to the size of microwell, the electric field is highly condensed in the free space, and both resistance and capacitance of the system increase accordingly.

### 3.5 Effect of anticancer drug

To test the sensibility of the tumor spheroid to anticancer drugs, a culture medium containing anticancer doxorubicin (DOX) was introduced into the lower chamber to simulate infusion treatment. DOX is an FDA-approved anthracycline chemotherapy drug, which inhibits cancer growth by binding to DNA-associated enzymes, disrupting cell division and proliferation.[35] U87 spheroids of 150  $\mu\text{m}$  in diameter were generated in the hydrogel microwells after incubation for 24 h in a serum-free culture medium. In reference to the previous studies, a DOX concentration of 5, 10, and 15  $\mu\text{g/ml}$  was applied respectively for a culture period of 40 h (Fig. 6). With the increase of the DOX concentration, some cells detached from the spheroids and the spheroids even collapsed at the highest DOX concentration (Fig. 6a). This can be quantified by calculating the ratio ( $\eta$ ) of the tumor spheroid projection area to the combined area of the tumor spheroid and the free cells nearby (Fig. 6b). Our results showed that  $\eta$  decreased with the increase of DOX concentration (Fig. 6c), meaning also an important lateral spreading and perhaps a decrease of the height of spheroids. To evaluate the cytotoxicity of DOX, a live/dead cell viability assay was performed using Calcein-AM and Propidium iodide (PI)-based fluorescence, showing a notable decline in cell viability with the increase of DOX concentration (Fig. 6d and 6e).

Impedance spectroscopy reveals a dose-dependent response in tumor spheroids to the anticancer drug (Fig. 6f and 6g). Without drug, the impedance was highly stable. After introducing drugs, a gradual decrease in resistance and capacitance was observed for lower doses (5 and 10  $\mu\text{g/ml}$ ) but a sharp decline in both resistance and capacitance was evidenced at 15  $\mu\text{g/ml}$ . Note also that at 15  $\mu\text{g/ml}$  the decrease of the resistance was earlier than that of the capacitance, suggesting a rapid dissociation of the spheroid which led to an increase of cell-free space and significant cell damage. This proves the concept of impedance monitoring of the response of tumor spheroids to anticancer drugs.

### 3.7 Influence of electric stimuli

An electric field may activate the voltage-gated ion channels of the cell membrane, leading to molecular movement and concentration rebalancing in the cell[36] and changes in cell adhesion and compactness of the spheroid (Fig. 7a). Consequently, drugs might more easily

penetrate into the spheroid. To assess the tumor sensitivity to the electric field, brief AC electric pulses at 500 Hz were administered. Fig. 7b illustrates the voltage pulse profile and the response of the tumor spheroids at 95 Hz as a function of time. When the spheroids were exposed to 0.1 V pulses for 10 s, no significant changes were observed. When the pulse amplitude increased to 0.2 V, the impedance exhibited detectable alterations. When the pulse amplitude increased to 0.3 V, the impedance experienced a sharp decline and then a progressive recovery to the initial level after 20 min. When the pulse amplitude reached 0.5 V, however, the impedance steadily increased over a period of 40 min. Finally, 0.2 V pulses were used to study enhanced drug effects. Ethylenediaminetetraacetic acid (EDTA) was chosen as a biochemical agent to remove calcium ions that are required to maintain cell adhesion as well as spheroid organization. Three assays were selected: (1) electrical stimulation alone (0.2V, AC 500Hz), (2) incubation with EDTA alone, and (3) incubation with EDTA in the presence of electrical pulses (Fig. 7c). To facilitate cell disassembly, the regular calcium-containing culture medium was replaced by a calcium-free medium with or without 2 or 4 mM EDTA. The impact on tumors was assessed by measuring the diameter of the spheroids (Fig. 7d and Fig. S9). When EDTA was combined with electric pulses, the effect was significantly enhanced, resulting in faster spheroid dissociation and cell detachment (Fig. 7e-f). We found that the electrical pulses alone had limited effects on the resistance of the system due to the stability of the spheroids (blue line). However, when the electrical stimulation and EDTA were applied simultaneously, the resistance of the system decreased remarkably and this effect was more pronounced with the increase of the EDTA concentrations.

Tumor spheroids are built up with tumor cells involving cell-cell interaction and cell interaction with the extracellular matrices. Under the influence of electric field, the spheroids can be fragilized due to the response of individual cells as well as the re-organization of the cells. Typically, cells are more or less disassociated, allowing a more efficient drug penetration.. Consequently, the diameter of the spheroid appears larger. However, this does not indicate an increase in resistance and capacitance. Since the number of cells does not increase and more electric field lines pass through the disrupted connections between cells, both resistance and capacitance actually decrease.

#### **4. Conclusion**

We have developed a new platform to study tumor spheroids on-a-chip. Uniform tumor spheroids were cultured and monitored in microwells of a suspended hydrogel membrane and under diffusion culture conditions. Our results showed that the size variation of the spheroids could be correlated to that of the electric resistance and capacitance of the system. Accordingly, the effect of anticancer drugs and applied electric fields could be studied. Recent studies have shown that different types of biomaterials could be engineered to facilitate spheroid formation[24,37–41] and various microfluidic devices could be used to regulate the tumor microenvironment.[9,14,15,42–49] The dynamic and diffusion-based culture presented in this work could be more relevant than static and perfusion-based culture. Co-culture of the tumor spheroids with other types of cells should be possible by using the present method.[31,50–53] Finally, it is easy to pattern a multi-electrode array on the glass slide so that it should be possible to apply the present method to measure the impedance of single spheroid and then to perform statistical analyses of the growth and the response to anticancer drugs of the tumor spheroids. With the growing interest in preclinical and clinical drug tests, more systematic investigations are expected.

#### **Ethics approval and consent to participate**

Not applicable.

#### **Consent for publication**

Not applicable.

#### **Availability of data and materials**

Not applicable.

#### **Competing interests**

The authors declare no conflict of interest.

#### **Funding**

This research was supported by the program Institut Carnot (IPGG Microfluidique N° 20 CARN 0037 01) and the program «Investissements d'Avenir» launched by the French Government and implemented by ANR with the references ANR-10-LABX-31 and ANR-10-IDEX-0001-02 PSL.

### **Authors' contributions**

W. W. and Y.L.: performed membrane fabrication, data acquisition, and analysis, X. H.: contributed to cell culture; F.L.: contributed impedance monitoring. H.L. and Z. M.: assisted membrane fabrication, L.W.: contributed to device preparation. J.P. and Y.C.: involved in planning and supervision. W.W. and Y.C. wrote the main manuscript text and prepared the figures. All authors discussed the results and reviewed the manuscript.

## Reference

1. Perche F, Torchilin VP. Cancer cell spheroids as a model to evaluate chemotherapy protocols. *Cancer Biology & Therapy*. 2012;13:1205–13.
2. Hanahan D. Hallmarks of Cancer: New Dimensions. *Cancer Discovery*. 2022;12:31–46.
3. Vakhshiteh F, Bagheri Z, Soleimani M, Ahvaraki A, Pournemat P, Alavi SE, et al. Heterotypic tumor spheroids: a platform for nanomedicine evaluation. *Journal of Nanobiotechnology*. 2023;21:249.
4. Hirschhaeuser F, Menne H, Dittfeld C, West J, Mueller-Klieser W, Kunz-Schughart LA. Multicellular tumor spheroids: An underestimated tool is catching up again. *Journal of Biotechnology*. 2010;148:3–15.
5. Costa EC, Moreira AF, de Melo-Diogo D, Gaspar VM, Carvalho MP, Correia IJ. 3D tumor spheroids: an overview on the tools and techniques used for their analysis. *Biotechnology Advances*. 2016;34:1427–41.
6. Moshksayan K, Kashaninejad N, Warkiani ME, Lock JG, Moghadas H, Firoozabadi B, et al. Spheroids-on-a-chip: Recent advances and design considerations in microfluidic platforms for spheroid formation and culture. *Sensors and Actuators B: Chemical*. 2018;263:151–76.
7. Nunes AS, Barros AS, Costa EC, Moreira AF, Correia IJ. 3D tumor spheroids as in vitro models to mimic in vivo human solid tumors resistance to therapeutic drugs. *Biotechnology and Bioengineering*. 2019;116:206–26.
8. Decarli MC, Amaral R, Santos DP dos, Tofani LB, Katayama E, Rezende RA, et al. Cell spheroids as a versatile research platform: formation mechanisms, high throughput production, characterization and applications. *Biofabrication*. 2021;13:032002.
9. Tevlek A, Kecili S, Ozcelik OS, Kulah H, Tekin HC. Spheroid Engineering in Microfluidic Devices. *ACS Omega*. 2023;8:3630–49.
10. Han SJ, Kwon S, Kim KS. Challenges of applying multicellular tumor spheroids in preclinical phase. *Cancer Cell International*. 2021;21:152.
11. Ota H, Yamamoto R, Deguchi K, Tanaka Y, Kazoe Y, Sato Y, et al. Three-dimensional spheroid-forming lab-on-a-chip using micro-rotational flow. *Sensors and Actuators B: Chemical*. 2010;147:359–65.
12. Ziółkowska K, Kwapiszewski R, Stelmachowska A, Chudy M, Dybko A, Brzózka Z. Development of a three-dimensional microfluidic system for long-term tumor spheroid culture. *Sensors and Actuators B: Chemical*. 2012;173:908–13.
13. Drost J, Clevers H. Organoids in cancer research. *Nat Rev Cancer*. 2018;18:407–18.
14. Sontheimer-Phelps A, Hassell BA, Ingber DE. Modelling cancer in microfluidic human organ-on-chips. *Nat Rev Cancer*. 2019;19:65–81.
15. Fang G, Chen Y-C, Lu H, Jin D. Advances in Spheroids and Organoids on a Chip. *Advanced Functional Materials*. 2023;33:2215043.
16. Flont M, Dybko A, Jastrzębska E. A layered cancer-on-a-chip system for anticancer drug screening

- and disease modeling. *Analyst*. 2023;148:5486–95.
17. Chen Z, Han S, Sanny A, Chan DL-K, van Noort D, Lim W, et al. 3D hanging spheroid plate for high-throughput CAR T cell cytotoxicity assay. *Journal of Nanobiotechnology*. 2022;20:30.
  18. Kwapiszewska K, Michalczuk A, Rybka M, Kwapiszewski R, Brzózka Z. A microfluidic-based platform for tumour spheroid culture, monitoring and drug screening. *Lab on a Chip*. 2014;14:2096–104.
  19. Edwards SJ, Carannante V, Kuhnigk K, Ring H, Tararuk T, Hallböök F, et al. High-Resolution Imaging of Tumor Spheroids and Organoids Enabled by Expansion Microscopy. *Frontiers in Molecular Biosciences* [Internet]. 2020 [cited 2023 Oct 8];7. Available from: <https://www.frontiersin.org/articles/10.3389/fmolb.2020.00208>
  20. Luongo K, Holton A, Kaushik A, Spence P, Ng B, Deschenes R, et al. Microfluidic device for trapping and monitoring three dimensional multicell spheroids using electrical impedance spectroscopy. *Biomicrofluidics*. 2013;7:034108.
  21. Thielecke H, Mack A, Robitzki A. A multicellular spheroid-based sensor for anti-cancer therapeutics. *Biosensors and Bioelectronics*. 2001;16:261–9.
  22. Curto VF, Ferro MP, Mariani F, Scavetta E, Owens RM. A planar impedance sensor for 3D spheroids. *Lab Chip*. 2018;18:933–43.
  23. Gong L, Petchakup C, Shi P, Tan PL, Tan LP, Tay CY, et al. Direct and Label-Free Cell Status Monitoring of Spheroids and Microcarriers Using Microfluidic Impedance Cytometry. *Small*. 2021;17:2007500.
  24. Kamatar A, Gunay G, Acar H. Natural and Synthetic Biomaterials for Engineering Multicellular Tumor Spheroids. *Polymers*. 2020;12:2506.
  25. Tang Y, Liu J, Chen Y. Agarose multi-wells for tumour spheroid formation and anti-cancer drug test. *Microelectronic Engineering*. 2016;158:41–5.
  26. Lee JM, Park DY, Yang L, Kim E-J, Ahrberg CD, Lee K-B, et al. Generation of uniform-sized multicellular tumor spheroids using hydrogel microwells for advanced drug screening. *Sci Rep*. 2018;8:17145.
  27. Li Y, Kumacheva E. Hydrogel microenvironments for cancer spheroid growth and drug screening. *Science Advances*. 2018;4:eaas8998.
  28. Kwisnek L, Goetz J, Meyers KP, Heinz SR, Wiggins JS, Nazarenko S. PEG Containing Thiol–Ene Network Membranes for CO<sub>2</sub> Separation: Effect of Cross-Linking on Thermal, Mechanical, and Gas Transport Properties. *Macromolecules*. 2014;47:3243–53.
  29. De Paz H, Chemtob A, Croutxé-Barghorn C, Le Nouen D, Rigolet S. Insights into Photoinduced Sol–Gel Polymerization: An in Situ Infrared Spectroscopy Study. *J Phys Chem B*. 2012;116:5260–8.
  30. Cavallo A, Madaghiele M, Masullo U, Lionetto MG, Sannino A. Photo-crosslinked poly(ethylene glycol) diacrylate (PEGDA) hydrogels from low molecular weight prepolymer: Swelling and permeation studies. *Journal of Applied Polymer Science* [Internet]. 2017 [cited 2023 May 30];134. Available from: <https://onlinelibrary.wiley.com/doi/abs/10.1002/app.44380>

31. Cuchiara MP, Allen ACB, Chen TM, Miller JS, West JL. Multilayer microfluidic PEGDA hydrogels. *Biomaterials*. 2010;31:5491–7.
32. Smyrek I, Mathew B, Fischer SC, Lissek SM, Becker S, Stelzer EHK. E-cadherin, actin, microtubules and FAK dominate different spheroid formation phases and important elements of tissue integrity. *Biology Open*. 2019;8:bio037051.
33. Zanoni M, Cortesi M, Zamagni A, Arienti C, Pignatta S, Tesei A. Modeling neoplastic disease with spheroids and organoids. *Journal of Hematology & Oncology*. 2020;13:97.
34. Luft C, Ketteler R. Electroporation Knows No Boundaries: The Use of Electrostimulation for siRNA Delivery in Cells and Tissues. *SLAS Discovery*. 2015;20:932–42.
35. Tacar O, Sriamornsak P, Dass CR. Doxorubicin: an update on anticancer molecular action, toxicity and novel drug delivery systems. *Journal of Pharmacy and Pharmacology*. 2012;65:157–70.
36. Taghian T, Narmoneva DA, Kogan AB. Modulation of cell function by electric field: a high-resolution analysis. *Journal of The Royal Society Interface*. 2015;12:20150153.
37. Wu Z, Chen B, Wu Y, Xia Y, Chen H, Gong Z, et al. Scaffold-free generation of heterotypic cell spheroids using acoustofluidics. *Lab Chip*. 2021;21:3498–508.
38. Kamei K, Koyama Y, Tokunaga Y, Mashimo Y, Yoshioka M, Fockenberg C, et al. Characterization of Phenotypic and Transcriptional Differences in Human Pluripotent Stem Cells under 2D and 3D Culture Conditions. *Advanced Healthcare Materials*. 2016;5:2951–8.
39. Wang B, Tu X, Wei J, Wang L, Chen Y. Substrate elasticity dependent colony formation and cardiac differentiation of human induced pluripotent stem cells. *Biofabrication*. 2018;11:015005.
40. Huang B, Peng J, Huang X, Liang F, Wang L, Shi J, et al. Generation of Interconnected Neural Clusters in Multiscale Scaffolds from Human-Induced Pluripotent Stem Cells. *ACS Appl Mater Interfaces*. 2021;13:55939–52.
41. Goodarzi S, Prunet A, Rossetti F, Bort G, Tillement O, Porcel E, et al. Quantifying nanotherapeutic penetration using a hydrogel-based microsystem as a new 3D in vitro platform. *Lab Chip*. 2021;21:2495–510.
42. Trujillo-de Santiago G, Flores-Garza BG, Tavares-Negrete JA, Lara-Mayorga IM, González-Gamboa I, Zhang YS, et al. The Tumor-on-Chip: Recent Advances in the Development of Microfluidic Systems to Recapitulate the Physiology of Solid Tumors. *Materials*. 2019;12:2945.
43. Zhang B, Korolj A, Lai BFL, Radisic M. Advances in organ-on-a-chip engineering. *Nat Rev Mater*. 2018;3:257–78.
44. Park SE, Georgescu A, Huh D. Organoids-on-a-chip. *Science*. 2019;364:960–5.
45. He Y, Huang B, Rofaani E, Hu J, Liu Y, Pitingolo G, et al. Fabrication of micro-cages and caged tumor spheroids for microfluidic chip-based assays. *Microelectronic Engineering*. 2020;225:111256.
46. Ma C, Peng Y, Li H, Chen W. Organ-on-a-Chip: A New Paradigm for Drug Development. *Trends in Pharmacological Sciences*. 2021;42:119–33.
47. He Y, Rofaani E, Huang X, Huang B, Liang F, Wang L, et al. Generation of Alveolar Epithelium

- Using Reconstituted Basement Membrane and hiPSC-Derived Organoids. *Advanced Healthcare Materials*. 2022;11:2101972.
48. Ingber DE. Human organs-on-chips for disease modelling, drug development and personalized medicine. *Nat Rev Genet*. 2022;23:467–91.
  49. Roth A, MPS-WS BERLIN 2019. Human microphysiological systems for drug development. *Science*. 2021;373:1304–6.
  50. Huang X, Liang F, Huang B, Luo H, Shi J, Wang L, et al. On-chip real-time impedance monitoring of hiPSC-derived and artificial basement membrane-supported endothelium. *Biosensors and Bioelectronics*. 2023;235:115324.
  51. Liang F, Huang X, Huang B, He Y, Luo H, Shi J, et al. A microfluidic tool for real-time impedance monitoring of in vitro renal tubular epithelial cell barrier. *Sensors and Actuators B: Chemical*. 2023;392:134077.
  52. Pitingolo G, He Y, Huang B, Wang L, Shi J, Chen Y. An automatic cell culture platform for differentiation of human induced pluripotent stem cells. *Microelectronic Engineering*. 2020;231:111371.
  53. Huang B, He Y, Rofaani E, Liang F, Huang X, Shi J, et al. Automatic differentiation of human induced pluripotent stem cells toward synchronous neural networks on an arrayed monolayer of nanofiber membrane. *Acta Biomaterialia*. 2022;150:168–80.

## Figure caption

**Figure 1.** Fabricated hydrogel microwell membrane. (a, b) SEM images of PDMS micro-posts with concave heads and their replica into a PEGDA hydrogel membrane. (c) Cross-section view of a microwell showing a concave bottom. (d) SEM image of a microwell showing more clearly the thin bottom layer.

**Figure 2.** Microfluidic system for dynamic and diffusion-based culture and impedance monitoring of tumor spheroids. (a) Schematic diagram of the system and flow circuit with growing tumor spheroids in microwells of a chip integrated hydrogel membrane. (b) Photographs of the setup, showing a chip flow controller, a multichannel impedance analyzer, a microfluidic device (chip), and a 50 ml reservoir.

**Figure 3.** Tumor spheroids in microwells of a hydrogel membrane. (a) Microscopic images of the tumor spheroids cultured under microfluidic conditions for 12 days, Scale bar: 250 $\mu$ m. (b) Statistics of cell distribution with different cell seeding numbers. (c) Diameter changes of the spheroids during 12 days. (d) Changes in cell number and spheroid volume during 12 days. (e) Fitting curves of growth data with both Gompertz and logistic models. A cell seeding number of 30, 60, and 120 was used to fit the data obtained with 20k, 40k, and 80k U87 cells. (f) SEM images of tumor spheroids in microwells. (g) Spheroid diameters in 6 randomly selected zones. (h) Spheroid circularity of the spheroids. The circularity of a square (0.785) and a triangle (0.604) are also shown.

**Figure 4.** Tumor spheroids in microwells of a hydrogel membrane. (a, b) SEM images showing details of cell aggregation. Scale bar: 200  $\mu$ m, 50  $\mu$ m, and 10 $\mu$ m, respectively. (c) Representative confocal images of immunofluorescent stained nuclei (blue), Ki67 (red), and F-actin (green). Scale bar: 50 $\mu$ m. (d) Fluorescence images of the spheroids after live/dead cell staining, Scale bar: 150 $\mu$ m.

**Figure 5.** Impedance monitoring of growing tumor spheroids in hydrogel microwells of a membrane. (a) Equivalent electric circuit of the device with an integrated membrane and growing tumor spheroids before and after normalization. (b) Contribution of different items of the system to the impedance spectrum. (c) Recorded impedance spectra before and after culture

for 12 days. (d, e) Deduced resistance and capacitance of growing tumor spheroids in microwells for 12 days.

**Figure 6.** Effect of anticancer drug to the tumor spheroids. (a) Phase images of the spheroids before and after DOX treatment for 40 h. Scale bar: 250  $\mu\text{m}$ . (b) Schematic diagram explaining the calculation of the ratio ( $\eta$ ) between the tumor spheroid projection area and the total area of the tumor spheroid with detached cells. (c) Ratio comparison of the tumor spheroids before and after DOX treatment, a total of 30 spheroids from 3 different experiments were counted in each group. (d) Fluorescence images of the spheroids after live/dead cell staining, Scale bar: 90  $\mu\text{m}$ . (e) Viability comparison of the spheroids before and after DOX treatment, and (f, g) Deduced resistance and capacitance of the tumor spheroids as a function of time, showing the dose effect of DOX treatment.

**Figure 7.** Effect of low voltage AC electric fields. (a) Schematic diagram to illustrate the effect of electric pulses on EDTA penetration. (b) Signals of stimulating pulses with different voltage amplitudes and variation of the system at 95 Hz. (c) Sequences of the treatment: i) electrical stimulation alone (0.2V), ii) sequential incubation with a medium containing 2 ml and 4 mM EDTA, and iii) the same as ii) except electric stimulation. (d) Ratio comparison after EDTA treatment with or without electric stimulation, a total of 30 spheroids from 3 different experiments were counted for each group of data (e, f) Variation of the system resistance and capacitance as a function of time, showing the effect of different stimuli.

# TOC

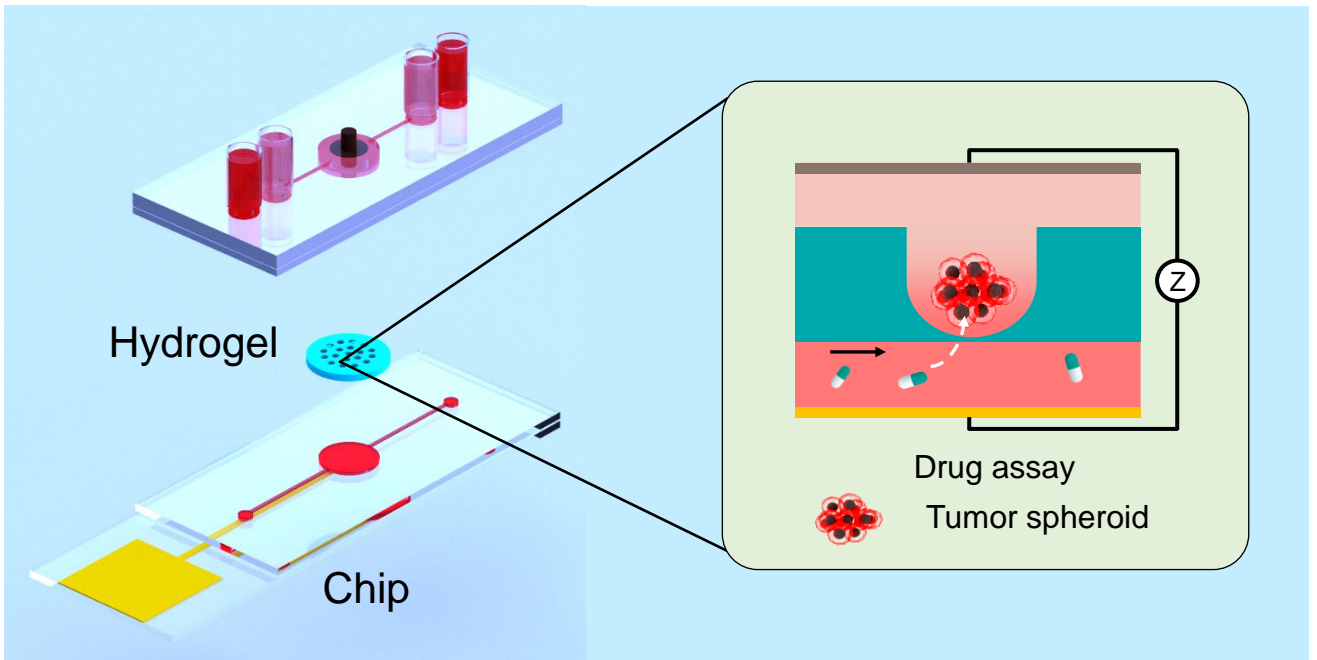


Fig. 1

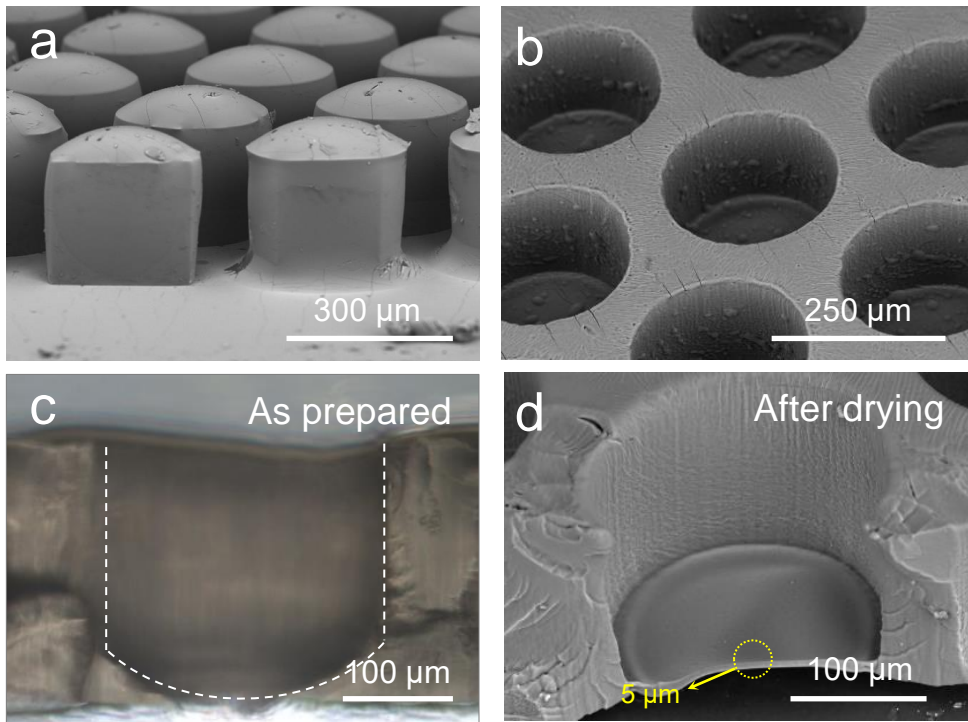


Fig. 2

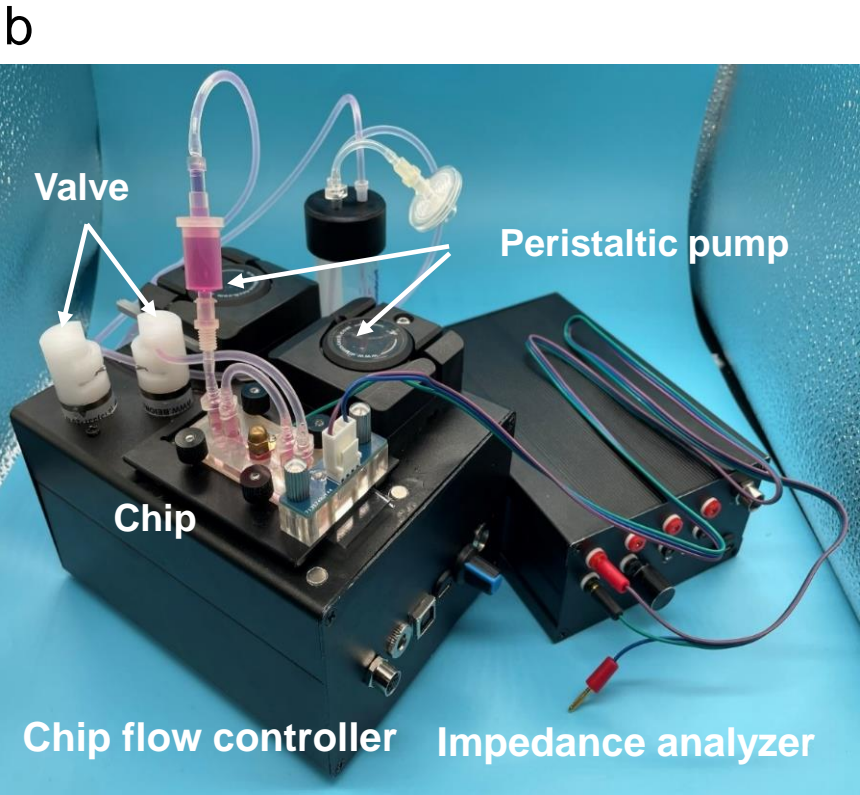
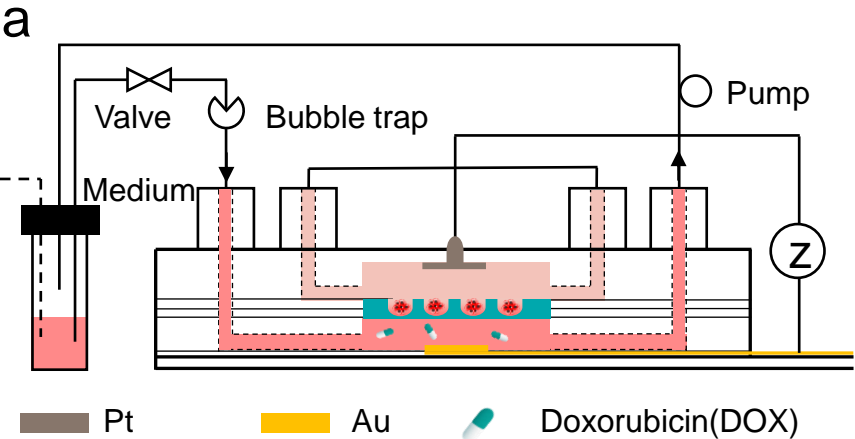


Fig. 3

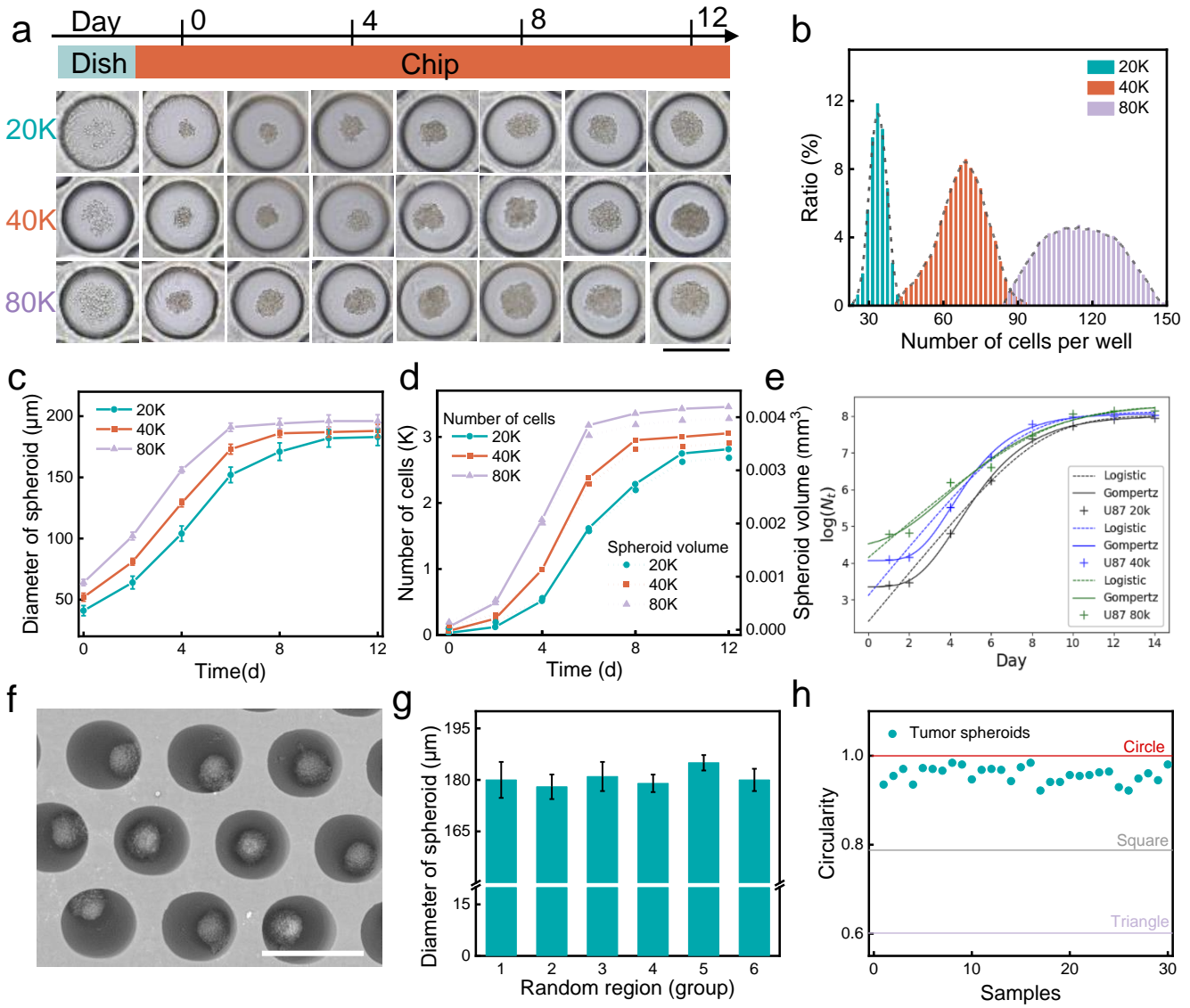


Fig. 4

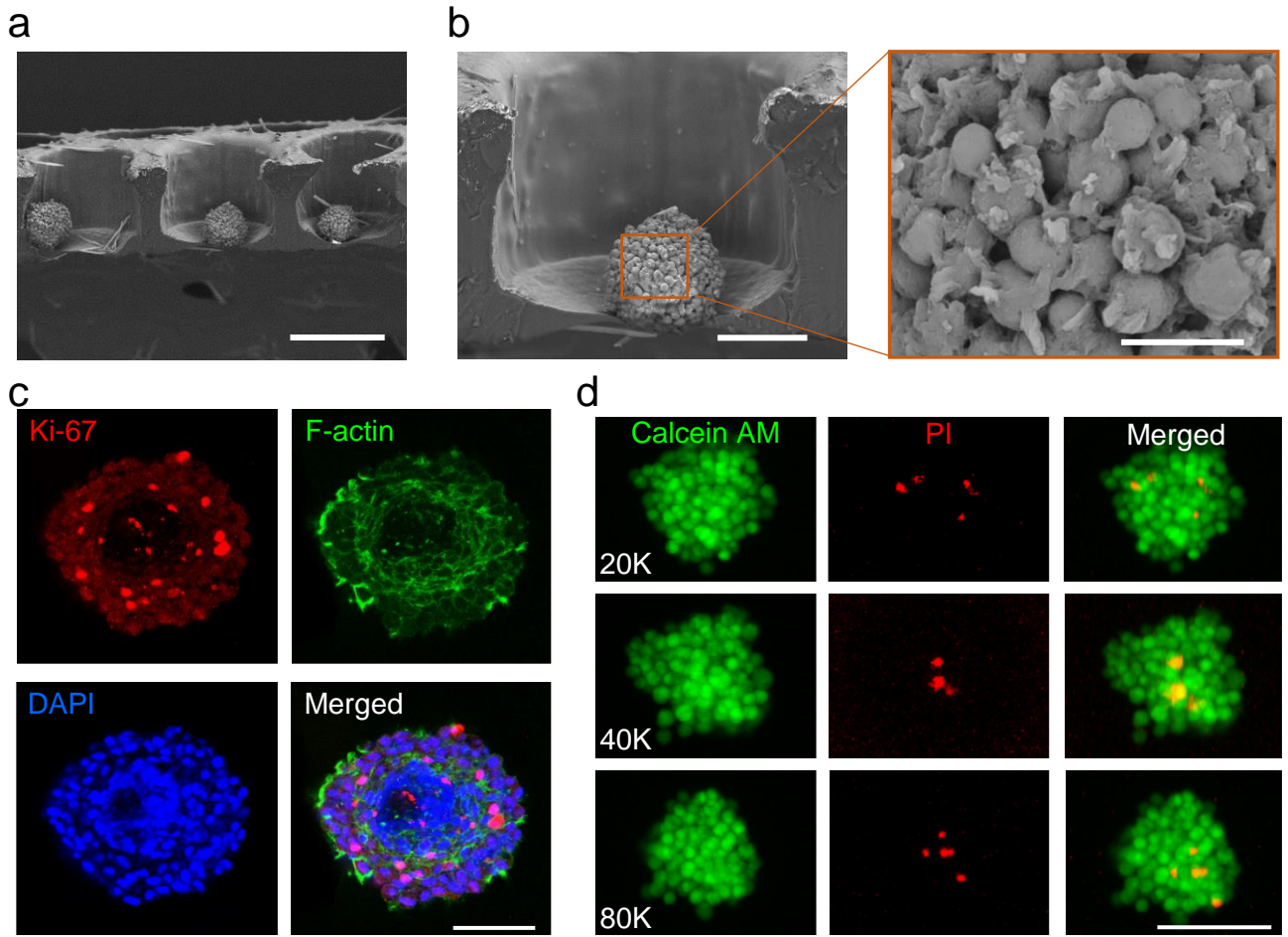


Fig. 5

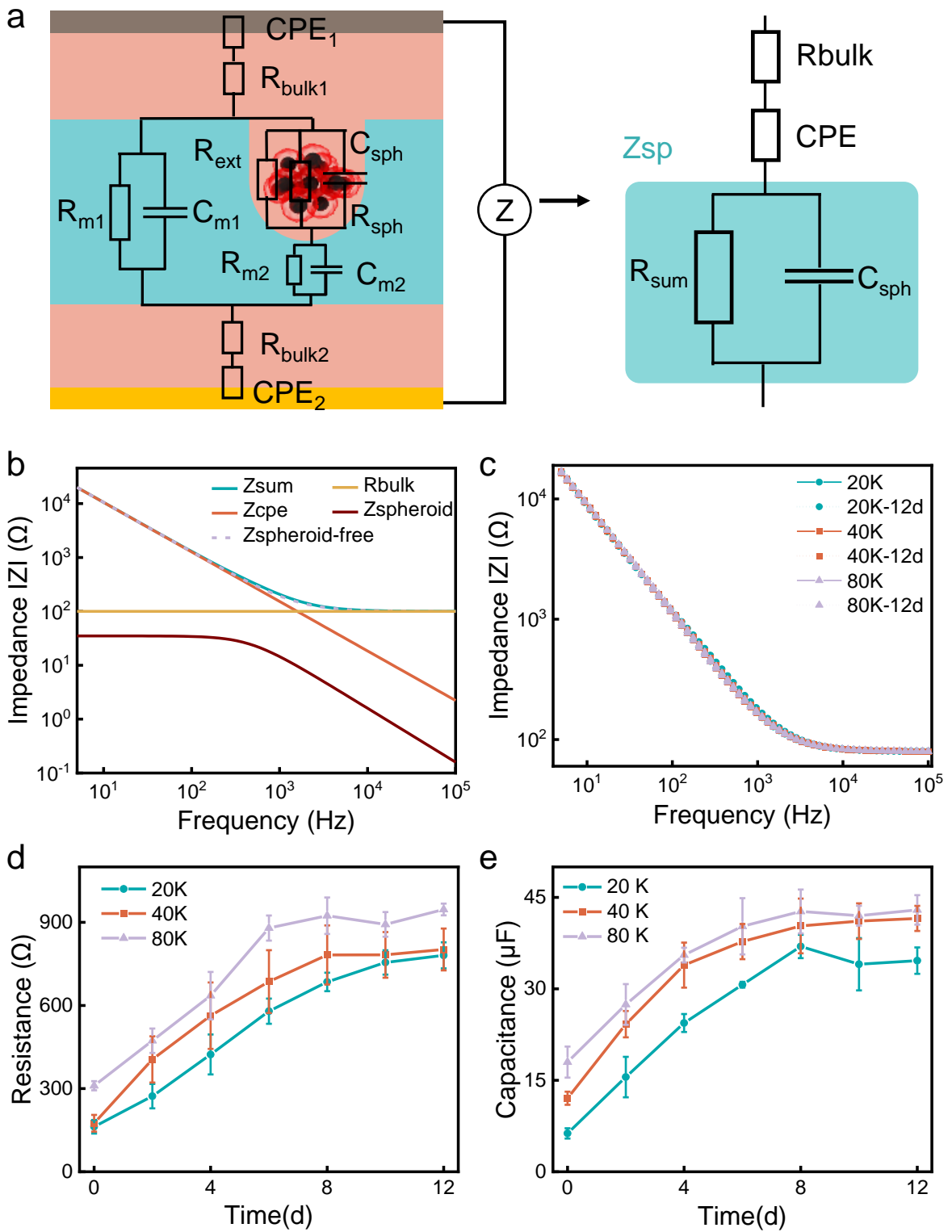


Fig. 6

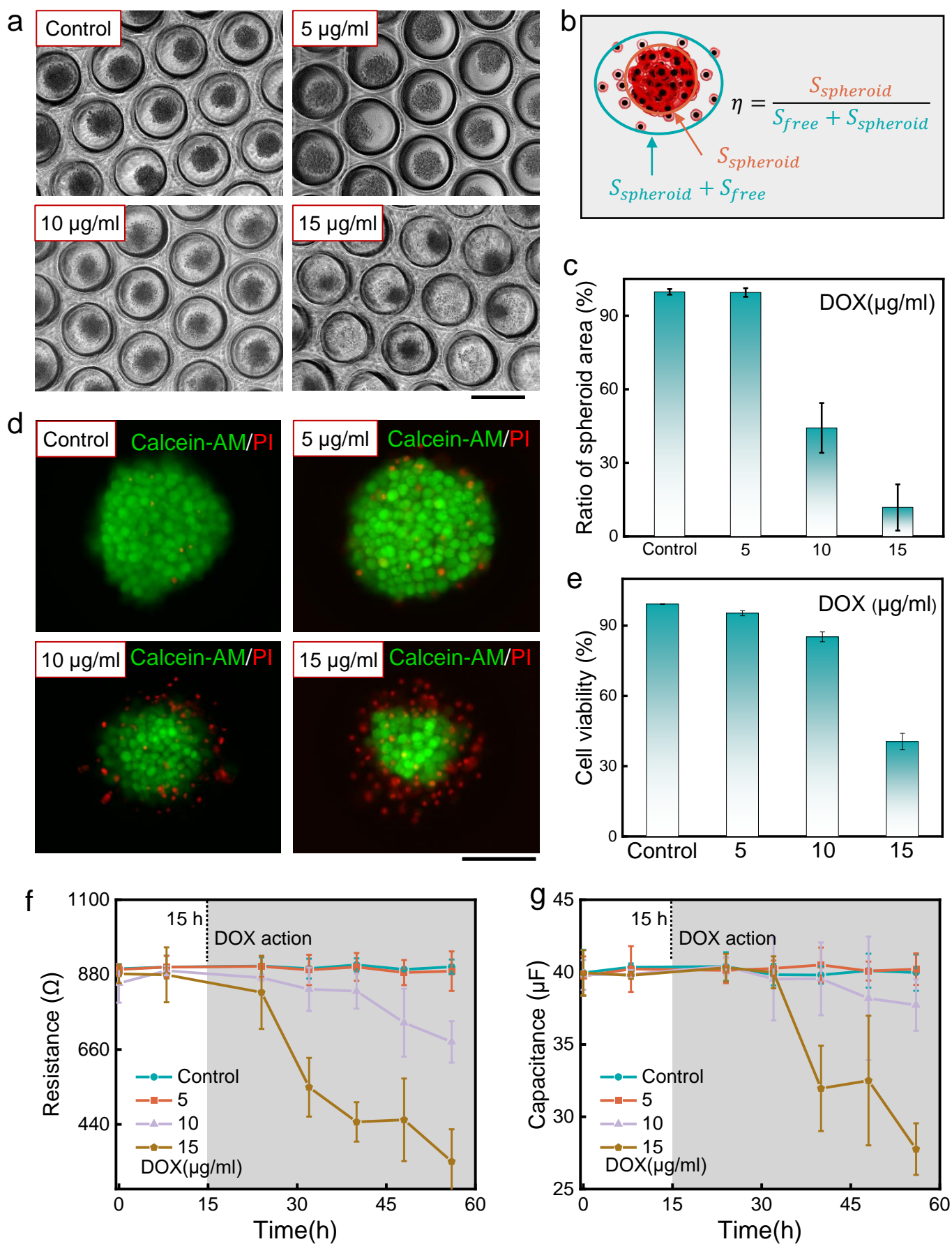


Fig. 7

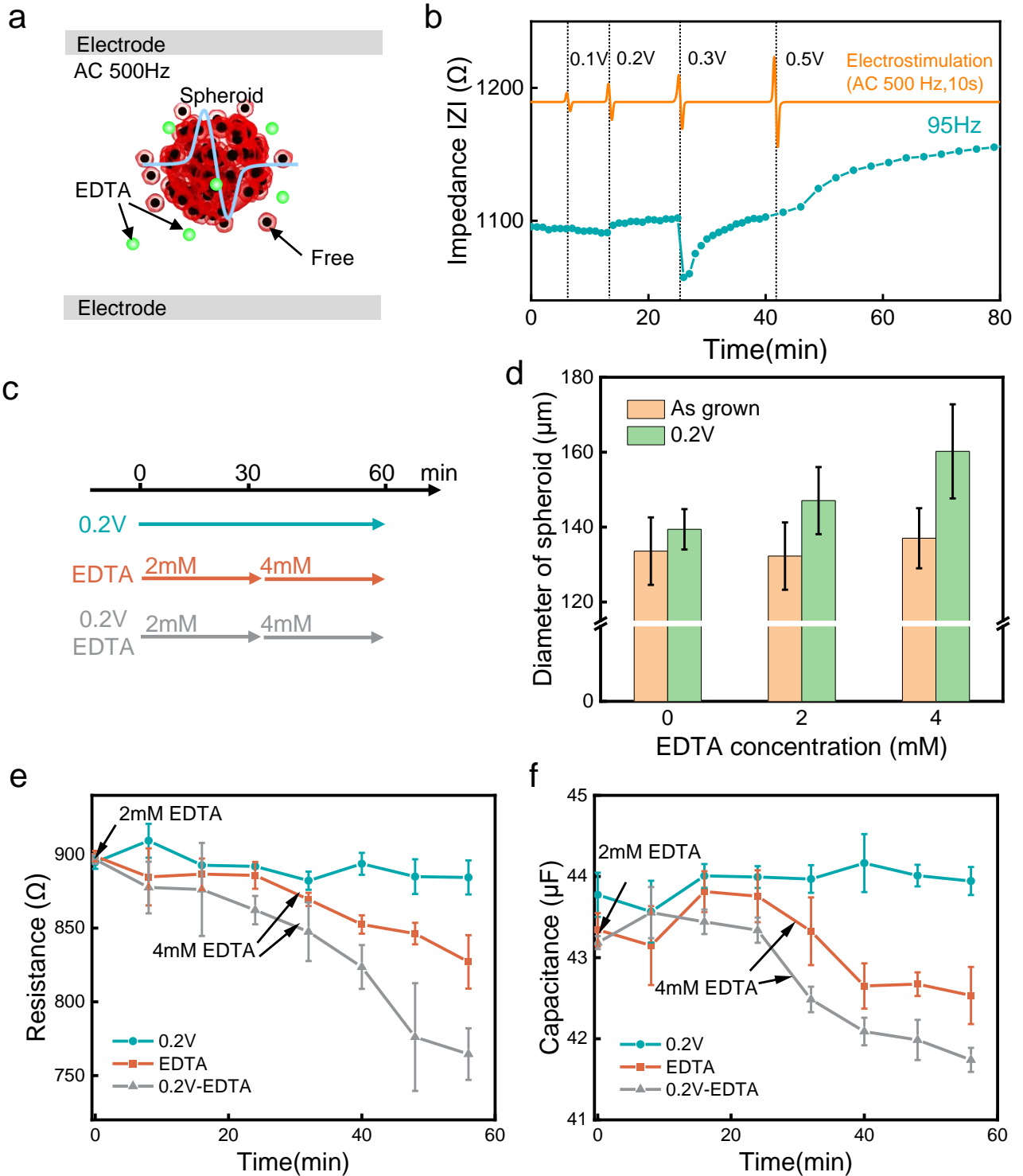


Fig. S1

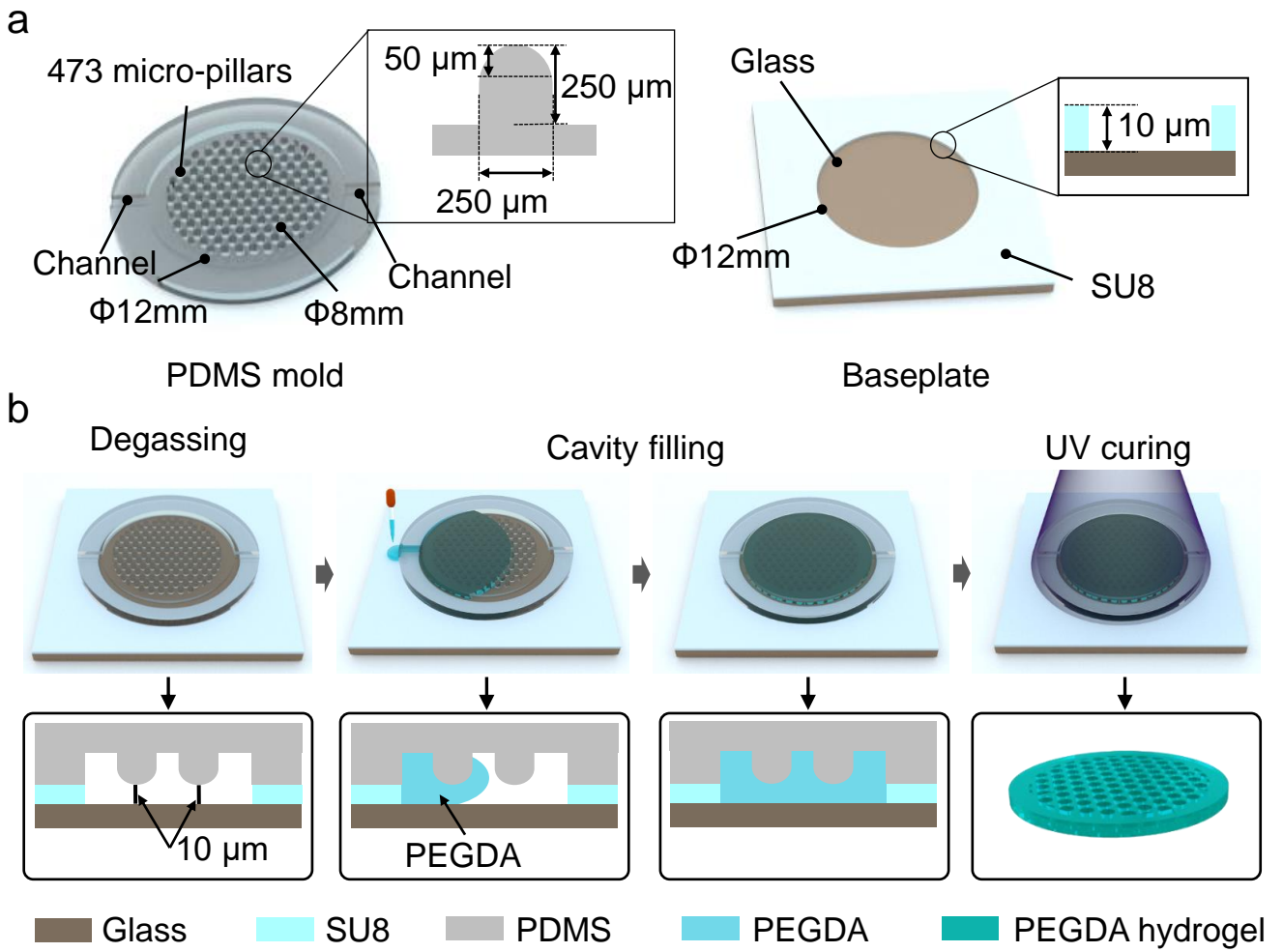
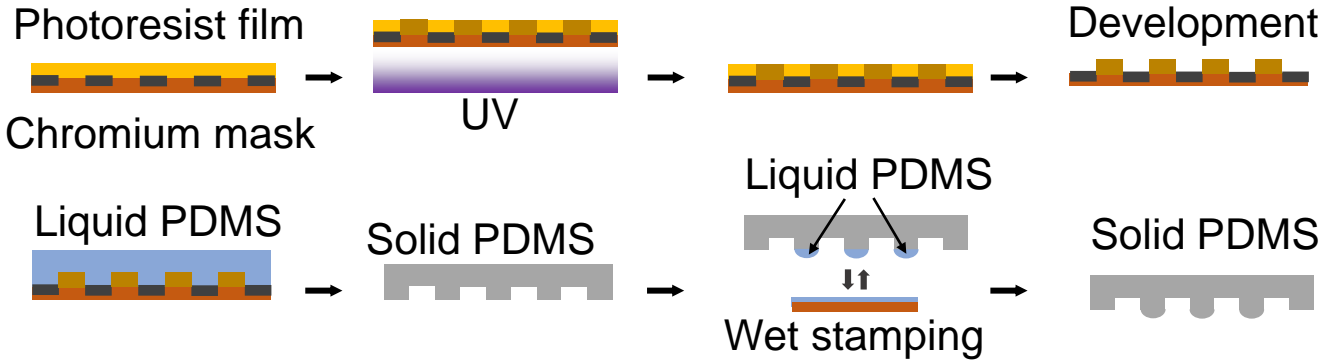


Fig. S2

### PDMS mold



### Baseplate

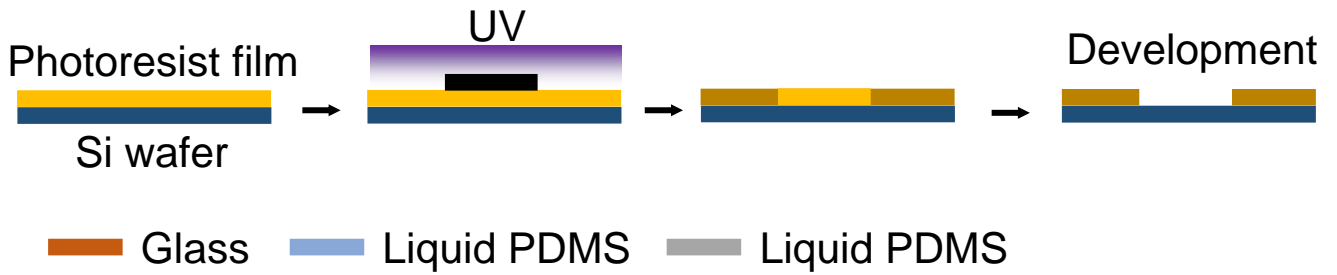
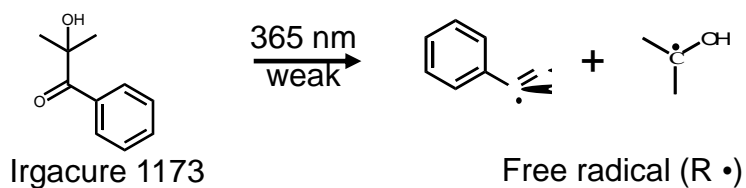
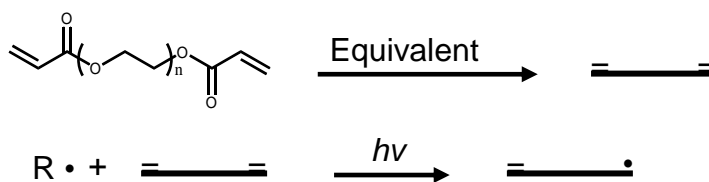


Fig. S3

a Step 1. Dissociation of the photoinitiator



Step 2. Radical initiation



Step 3. Network formation

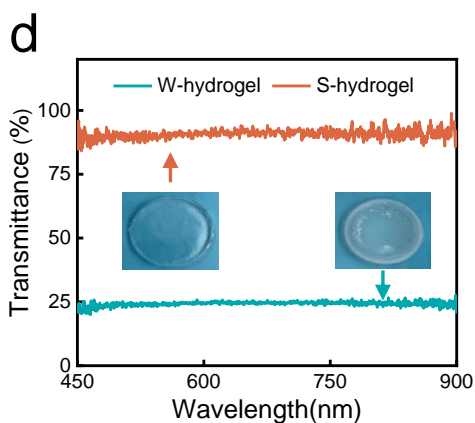
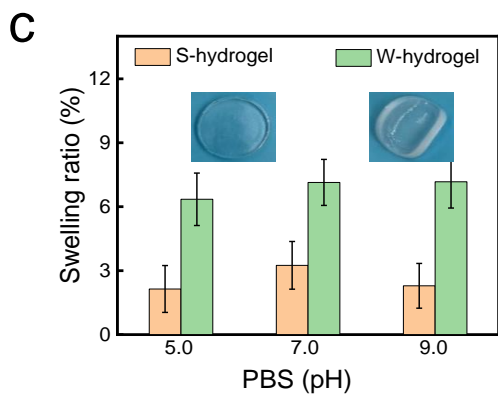
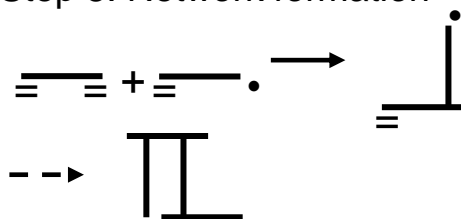


Fig. S4

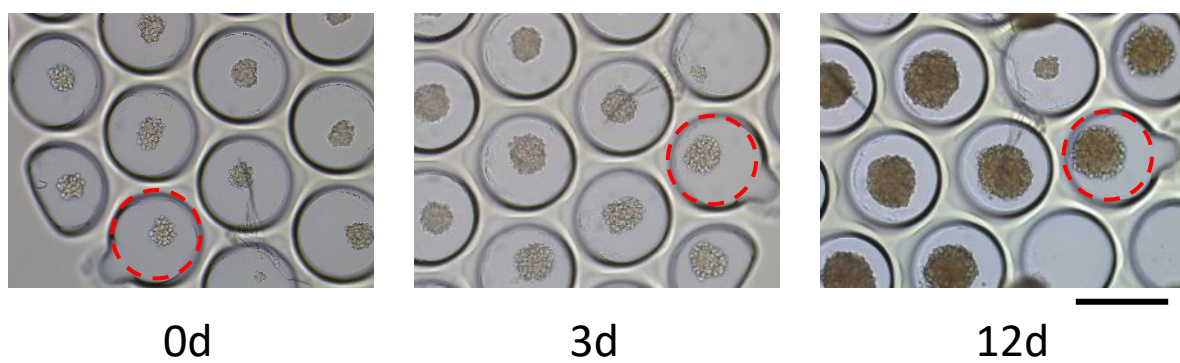


Fig. S5

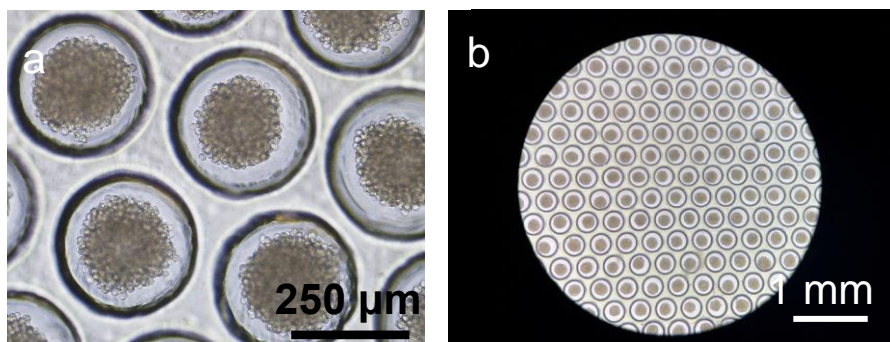


Fig. S6

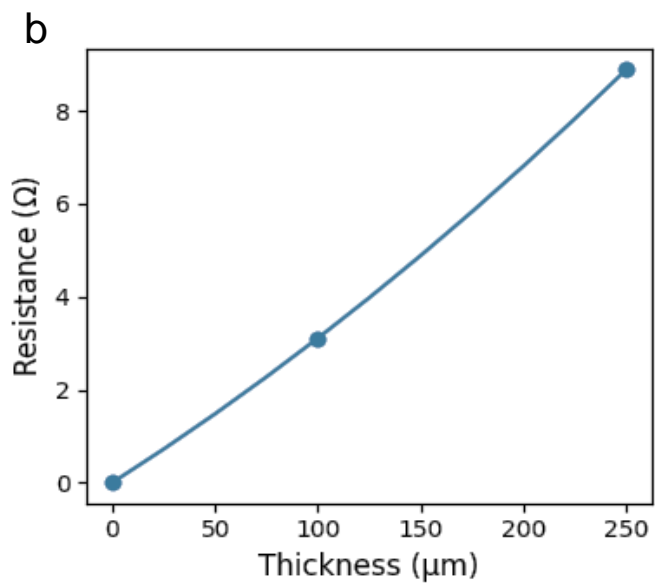
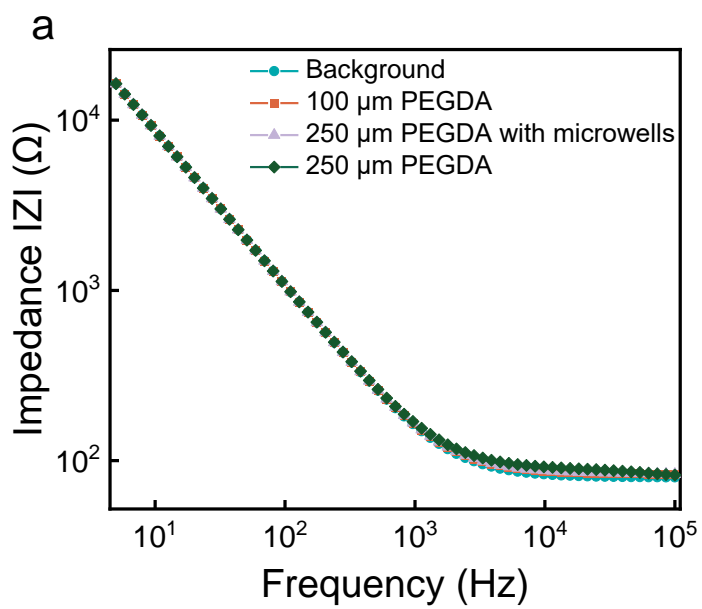


Fig. S7

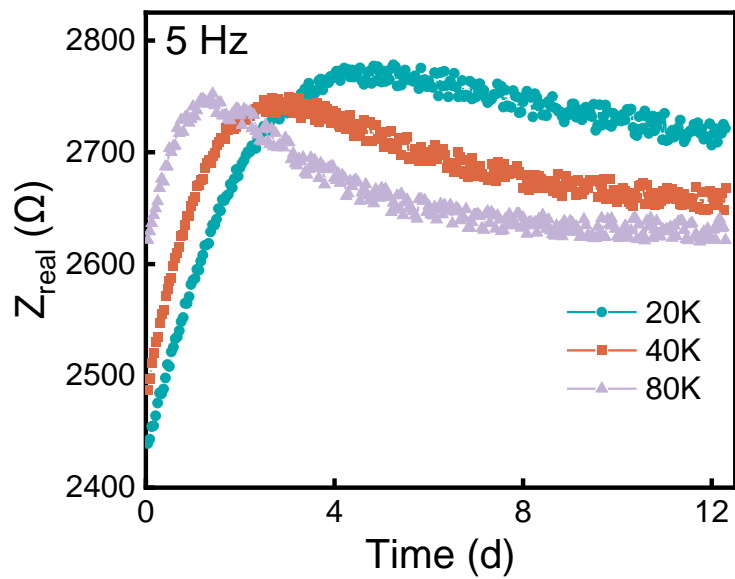
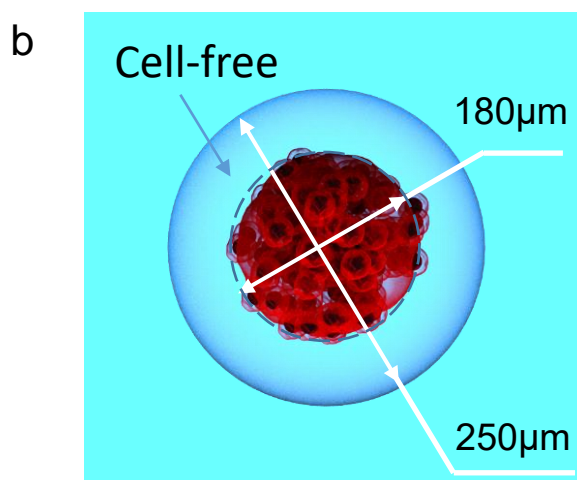
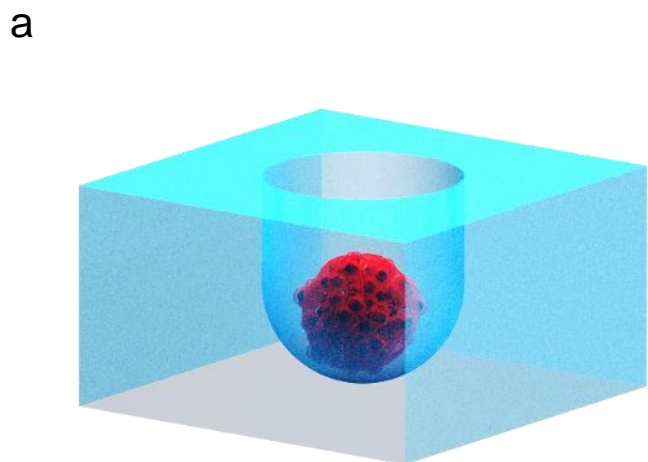
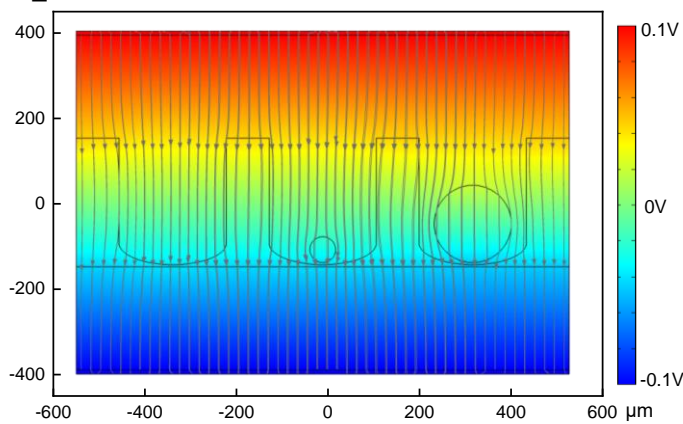


Fig. S8



c

$\Xi$  Surface: electric potential, Filament line: electric field



d

$\Xi$  Surface: electric potential, Filament line: electric field

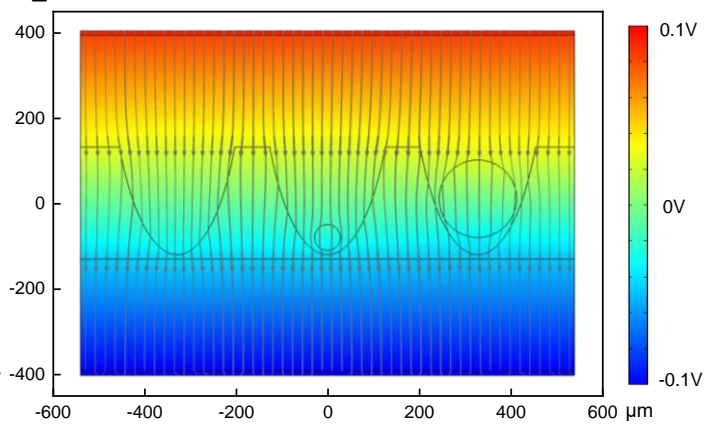
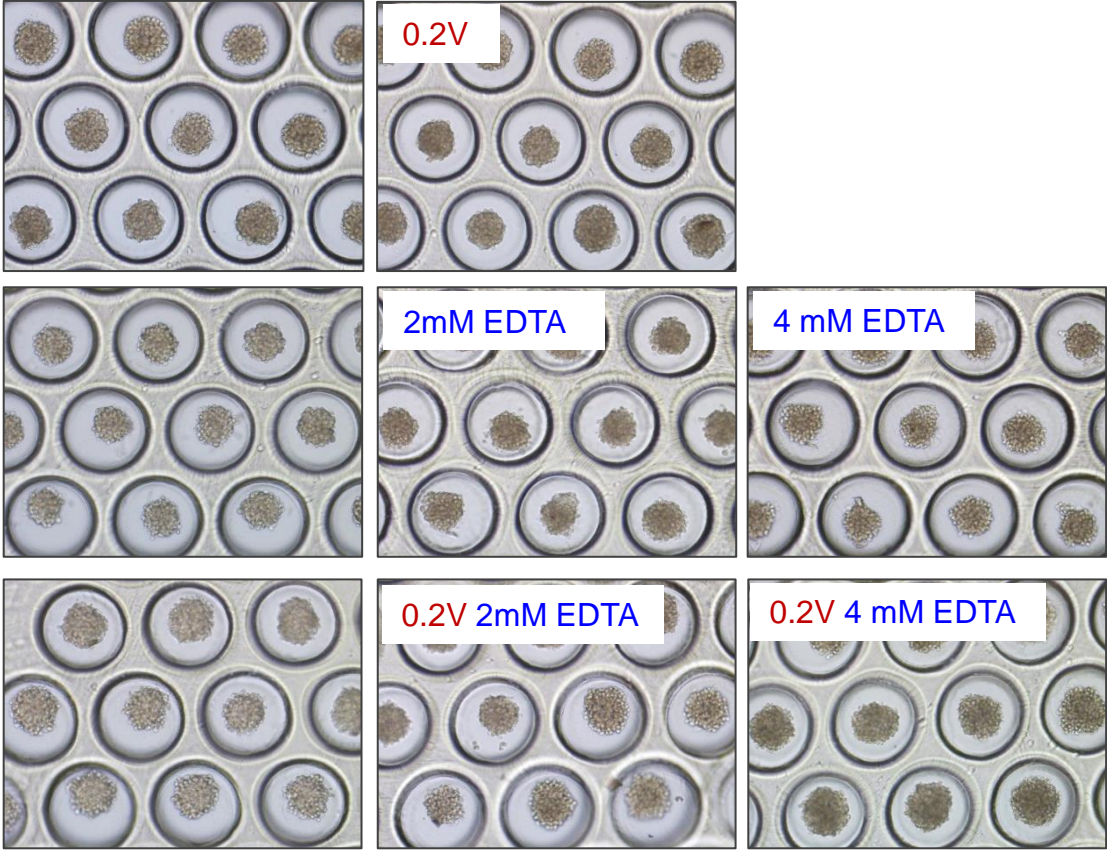


Fig. S9



## Supplementary Information

### Diffusion-based culture and real-time impedance monitoring of tumor spheroids in hydrogel microwells of a suspended membrane under microfluidic conditions

*Wei Wang<sup>a,1</sup>, Yuanhui Liu<sup>b,c,1</sup>, Xiaochen Huang<sup>a</sup>, Feng Liang<sup>a</sup>, Haoyue Luo<sup>a</sup>, Zheng Mao<sup>a</sup>, Li Wang<sup>d</sup>, Juan Peng<sup>a\*</sup>, Yong Chen<sup>a\*</sup>*

*<sup>a</sup> École Normale Supérieure-PSL Research University, Département de Chimie, Sorbonne Universités-UPMC Univ Paris 06, CNRS UMR 8640, PASTEUR, 24, rue Lhomond, 75005 Paris, France*

*<sup>b</sup> Department of Oncology, Tongji Hospital, Tongji Medical College, Huazhong University of Science and Technology, Wuhan 430030, Hubei, China*

*<sup>c</sup> Cancer Center, Tongji Hospital, Tongji Medical College, Huazhong University of Science and Technology, Wuhan, 430030, Hubei, China.*

*<sup>d</sup> MesoBioTech, 231 Rue Saint-Honoré, 75001, Paris, France*

*<sup>1</sup> These authors have equal contributions*

*E-mail : [yong.chen@ens.psl.eu](mailto:yong.chen@ens.psl.eu), [juan.wang@ens.psl.eu](mailto:juan.wang@ens.psl.eu)*

#### Inventory of Supplementary Information

Supplementary methods

Table 1

Figure S1-S9

## Supplementary Methods

### 1. Flow parameters of the culture medium

In a microfluidic chamber, the culture medium has to be renewed continuously or periodically to provide sufficient nutrients and prevent excessive accumulation of metabolites. In the case of tumor spheroids, the renewal depends on the size and properties of the spheroids as well as the specifications of the device. In this work, a hydrogel microwell membrane was used which is highly permeable so that the exchange of nutrients and wastes can be done mostly with the lower chamber across the thin bottom layer of the microwells. For the convenience of processing, the culture medium was renewed once per hour. To estimate the glucose and oxygen consumption of the plateau phase tumors, 3000 cells per well can be considered (Fig. 3e), corresponding to a total number of  $\sim 1.4$  M cells on the membrane. Assuming further that the number of dead cells is negligible and all cells contribute equally to the metabolic activities of the tumors. With a glucose (oxygen) consumption rate of  $1 \times 10^{-16} \text{ mol/cell.s}$  ( $1 \times 10^{-17} \text{ mol/cell.s}$ ), [1] a consumption rate of  $\sim 3.5 \text{ } \mu\text{mol/h}$  ( $\sim 0.35 \text{ } \mu\text{mol/h}$ ) can be estimated for all tumor cells in the wells. Considering a culture medium with a glucose (oxygen) concentration of 25 mM (0.18 mM) [2] and a chamber volume of 200  $\mu\text{L}$ , the quantity of glucose (oxygen) in the low chamber is then 5  $\mu\text{mol}$  (0.4  $\mu\text{mol}$ ). This means that a renewal rate of once per hour (5  $\mu\text{mol}$  glucose and 0.4  $\mu\text{mol}$  oxygen) is sufficient to compensate for the consumption of the spheroids (3.5  $\mu\text{mol}$  glucose and 0.35  $\mu\text{mol}$  per hour) in the microwells.

## 2. Calculation of size-dependent impedance

The impedance of the hydrogel microwell membrane with growing tumor spheroids can be calculated as follows

$$\frac{1}{Z} = \frac{1}{Z_0} + \sum_N \frac{1}{Z_w} = \frac{1}{Z_0} + \frac{N}{Z_w} \quad (1)$$

where  $Z_w$  is the impedance of the spheroid containing single wells,  $N$  is the number of wells, and  $Z_0$  is the impedance of the remaining part outside the wells. For the given system, only  $Z_w$  needs to be considered since the thickness so the electric impedance of the area outside microwells are significantly larger than the remaining parts, i.e.  $Z_0 \gg Z_w$ .  $Z_w$  can be expressed by

$$\frac{1}{Z_w} = \frac{1}{Z_s} + \frac{1}{Z_f} \quad (2)$$

where  $Z_s$  is the impedance of the spheroid projection area, which can be calculated with an equivalent circuit of a spheroid resistance ( $R_s$ ), and a spheroid capacitance ( $C_s$ ) connected in parallel, and  $Z_f$  is the impedance of the free space outside of that area,

$$Z_f = \frac{\rho H}{\pi(D_w^2 - D^2)} \quad (3)$$

where  $\rho$  is the resistivity of the culture medium,  $D$  is the diameter of the cylinder, and  $D_w$  and  $H$  are respectively the diameter and depth of the well. To observe the size dependence of the system, a cylindric aggregate of cells can be used to approach the spheroid. For simplicity, the contribution above and below the cylinder can be neglected. If the cells are vertically coupled, only the outside membranes of the top and the bottom cell layers are effective, which gives rise

$$R_s = \left(\frac{l}{D}\right)^2 R_c \quad \text{and} \quad C_s = \left(\frac{D}{l}\right)^2 C_c \quad (4a,4b)$$

where  $R_c$  and  $C_c$  are the resistance and capacitance of single cells, and  $l$  measures the cell size. If the cells are vertically decoupled, one should have

$$R_s = \frac{l}{D} R_c \quad \text{and} \quad C_s = \frac{D}{l} C_c \quad (5a,5b)$$

Therefore,  $C_s$  and the system's capacitance increase with the size of the spheroid in both cases. Since the resistance of spheroid ( $R_s$ ) and that of the free-space ( $Z_f$ ) are connected in parallel and  $Z_f$  is significantly smaller than  $R_s$ ,  $R_w$  and the capacitance of the system also increase with the size of the spheroids, in qualitative agreement with the experimental observation.

### 3. Finite element analysis of the electric field distribution

Start with the following Poisson equation:

$$-\nabla(\varepsilon_r \varepsilon_0 \nabla V) = 0 \quad (1)$$

where  $V$  is the electric potential,  $\varepsilon_0$  is the dielectric constant in vacuum ( $8.86 \times 10^{-12}$  F/m),  $\varepsilon_r$  is the relative permittivity of the material and  $\nabla$  is the Laplace operator. The electric field is given by

$$E = -\nabla V \quad (2)$$

The problem can then be solved by setting a charge distribution under static conditions. The relative permittivity of both culture medium (78) and PEGDA (10) are known. Then, the permittivity of the PEGDA hydrogel can be calculated[3]

$$\varepsilon = \left[ \left( \frac{1}{\varepsilon_2^3} - \frac{1}{\varepsilon_1^3} \right) v_2 + \frac{1}{\varepsilon_1^3} \right]^3 \quad (3)$$

where  $\varepsilon_1$  and  $\varepsilon_2$  are the relative permittivity of two constituent materials (culture medium and PEGDA), and  $v_2$  is the volume fraction of the PEGDA (24%).

The numerical results can be calculated by using the finite element method which depends on the shape of the microwells, i.e., the boundary conditions of the system. For simplicity, a 2D model (Fig. S2) was considered with a terminal voltage of  $\pm 0.1$  V. By using COMSOL Multiphysics, the electric field lines could be plotted (Fig. S7). As can be seen, two types of microwells were considered, showing that the electric field lines in the PEGDA hydrogel region are sparser than those in the culture medium. The electric field lines in the microwells in the presence of a tumor spheroid could also be calculated, assuming a permittivity of 40 for the tumor spheroids [4]. In the presence of the spheroid, the electric field lines are reset, giving rise to a higher field strength in the microwell outside the spheroid. With the increase of the spheroid size, the electric field strength also increases. However, the increase of the electric field strength is more clearly pronounced in the microwell with a flatter bottom layer, which is in favor of impedance monitoring of the tumor spheroids.

**Table 1.** Fitting parameters using the least square method and an equivalent circuit of a system with or without a flat PEGDA membrane, in comparison with a membrane with microwells.  $A$ ,  $n$ ,  $R_{\text{bulk}}$ , and  $R_{\text{sum}}$  are defined in section 2.5,  $C_m$  is the capacitance of membrane.

Target	$A$ ( $s^{-n-1} \mu F/cm^2$ )	$n$	$R_{\text{bulk}}$ ( $\Omega$ )	$R_{\text{sum}}$ ( $\Omega$ )	$C_m$ ( $\mu F$ )
Background	2.61	0.91	79.57	-	-
100 $\mu m$ PEGDA	2.61	0.91	80.06	3.11	0.22
250 $\mu m$ PEGDA with microwells	2.61	0.91	79.72	4.31	0.23
250 $\mu m$ PEGDA	2.61	0.91	79.47	8.89	0.30

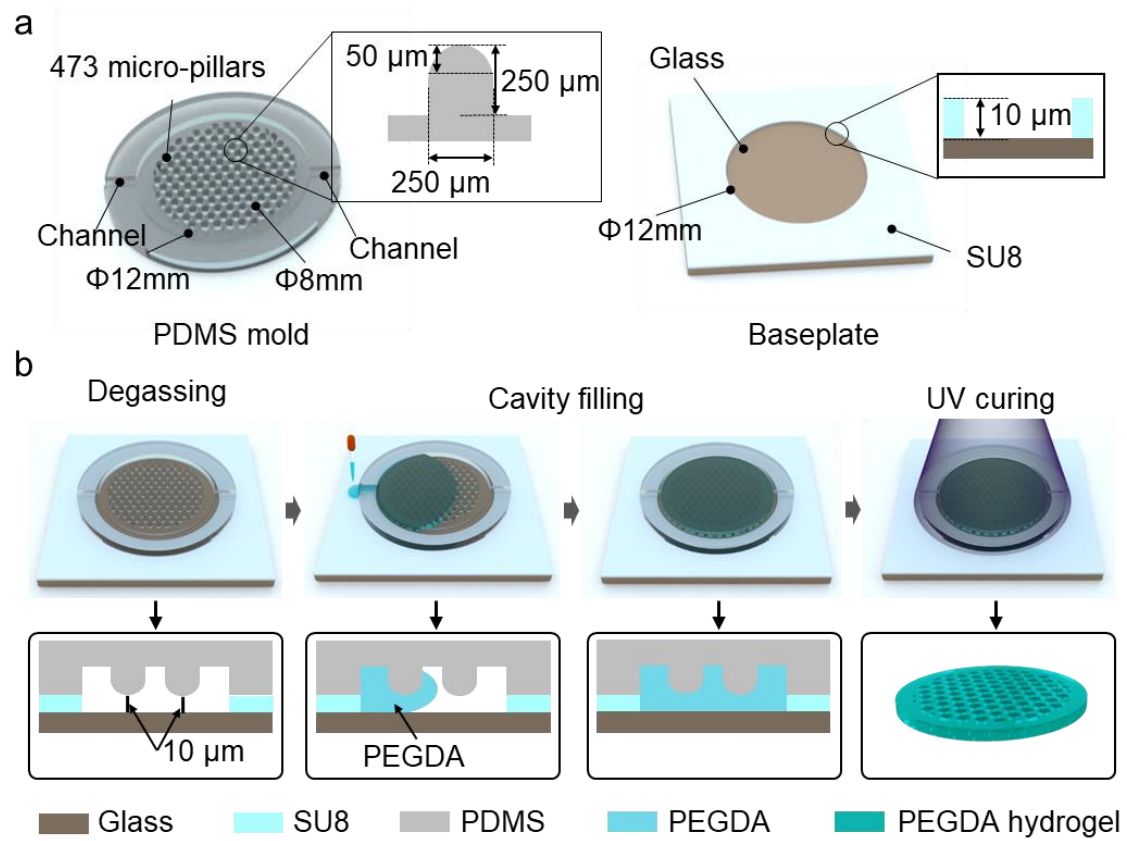
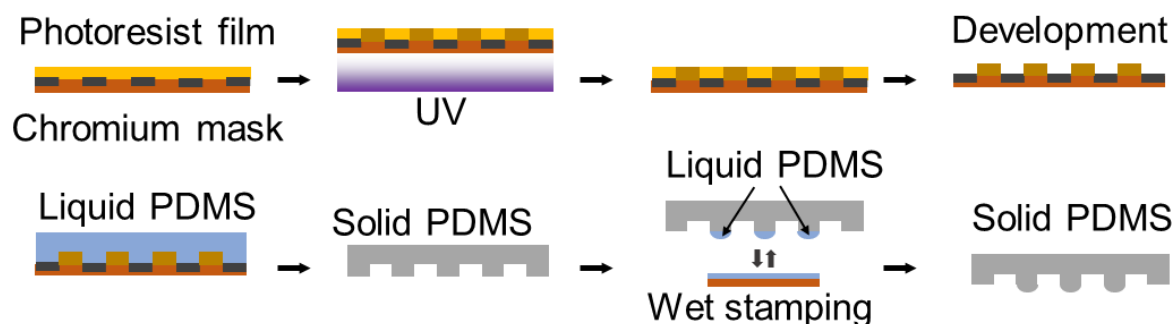


**Figure S1.** Fabrication of PEGDA microwell membrane. (a) Geometry parameters of the PDMS mold and the baseplate. (b) Steps of PEGDA molding: degassing, cavity filling, and UV curing.

## PDMS mold



## Baseplate

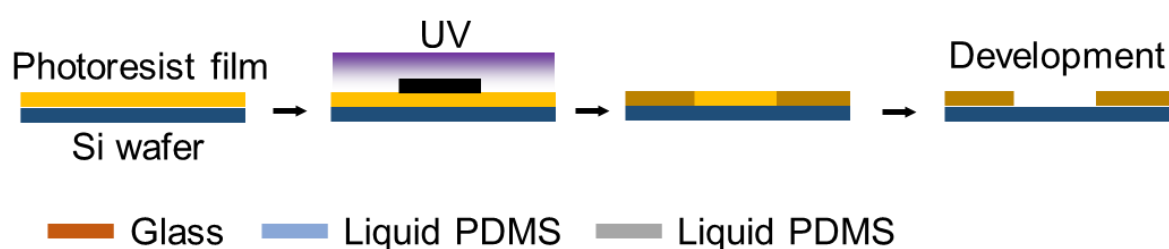


**Figure S2.** Fabrication steps of the PDMS mold and the baseplate for vacuum and UV-assisted molding. For the PDMS mold fabrication, a photoresist pattern is prepared by photolithography. After PDMS casting and thermal curing, a PDMS replica is obtained. To create a concave morphology at the end of the micro-posts of PDMS, the replica is brought into contact with a flat viscous PDMS (wet stamping). After curing, the PDMS mold is obtained. Photolithography is also used to define the baseplate.

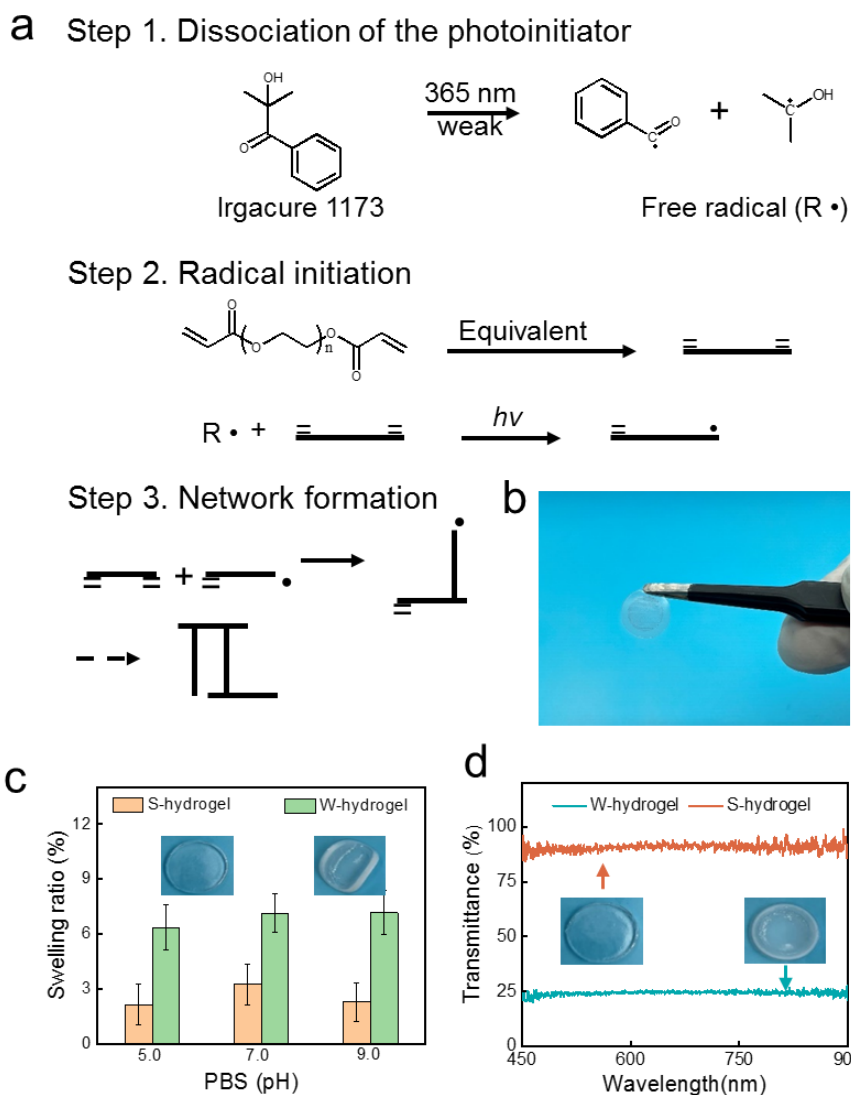


**Figure S3.** (a) Schematic diagram of chemical processes of UV curing of PEGDA. First, the photoinitiator molecules decompose into radicals under UV light. Then, the radical is initiated with monomers to form an active center, which leads to a continuous reaction through the carbon-carbon double bond on the macromers and the formation of a growing kinetic chain as well as a cross-linked network. Finally, a 3D hydrogel network is formed via radical chain polymerization. (b) Photograph of a fabricated hydrogel microwell membrane handled with a tweezer. (c) Swelling ratio of S-hydrogel and W-hydrogel in PBS of different pH values. Insert: Photographs of a PEGDA solution before and after UV curing. (d) Transmission spectra of S-hydrogel and W-hydrogel. Insert: Photographs of a S-hydrogel and a W-hydrogel membrane.

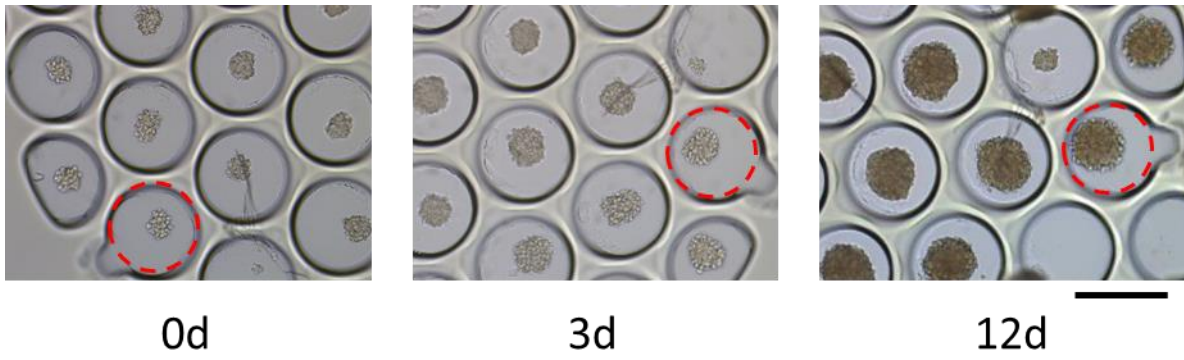


**Figure S4** Microphotographs of tumor spheroids in hydrogel microwells on a membrane under static culture conditions for 12 days are presented. The membrane was secured at the bottom of a 24-well plate, each well supplied with 200  $\mu\text{L}$  of culture medium. The medium was refreshed every two days, resulting in a cell proliferation rate comparable to that observed using a microchip. Scale bar: 250  $\mu\text{m}$ .

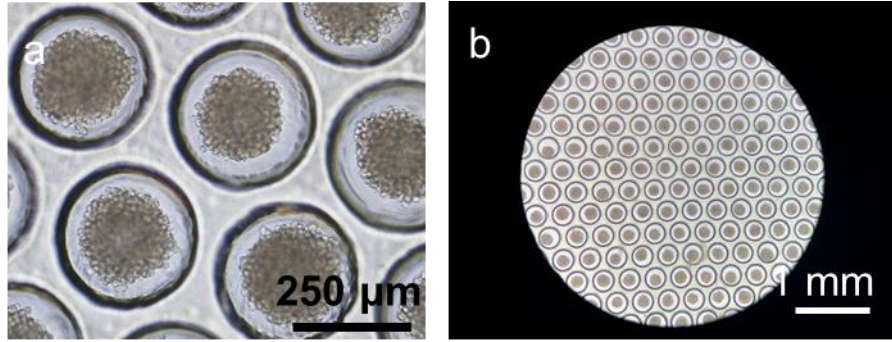


**Figure S5** (a) Microphotograph of tumor spheroids formed with a hydrogel microwell membrane. 160 K cells were seeded on the membrane. After culture for 4 days, larger tumor spheroids were observed in the microwells of the hydrogel membrane. (b) Microphotograph of tumor spheroids grown in a PEGDA microwell membrane, showing excellent size and form homogeneity of the spheroids.

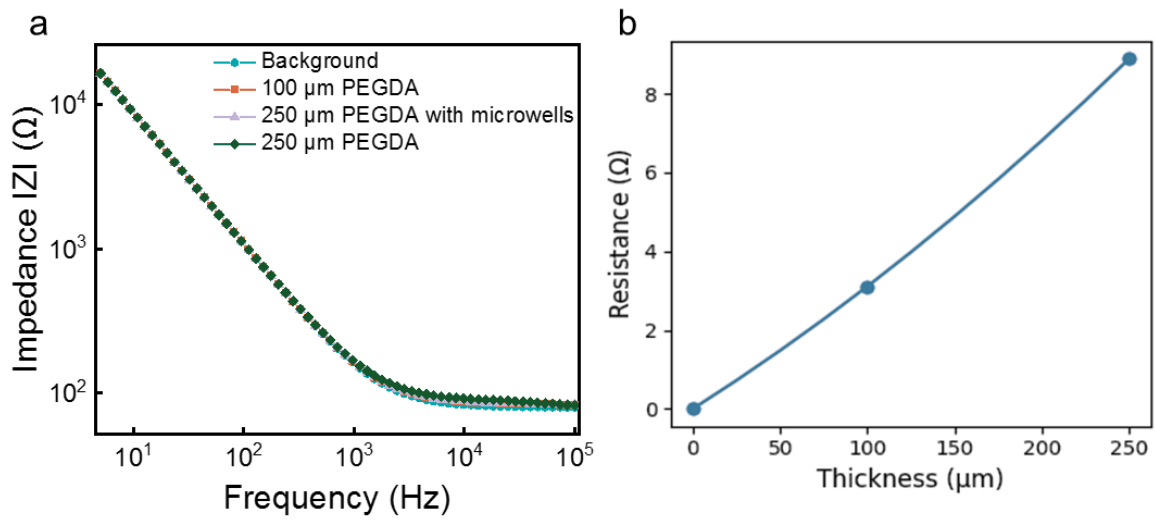


**Figure S6** (a) Impedance spectra of the system without membrane and with a flat PEGDA membrane of different thicknesses, in comparison with that of the membrane with microwells. (b) Deduced resistances of membranes of different thicknesses (dots) and their least square fitting curve (line).

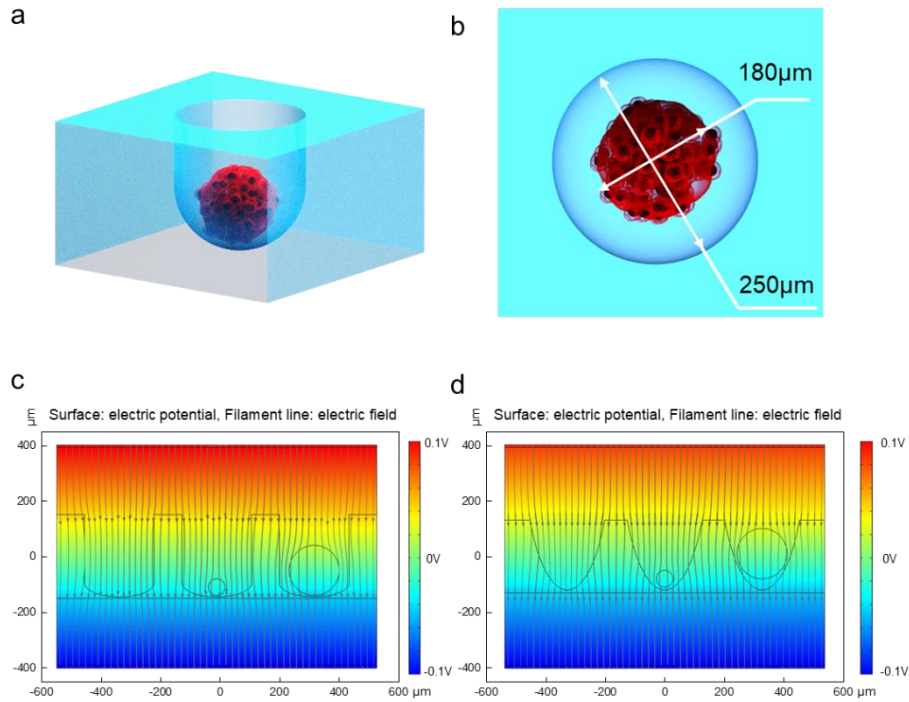


**Figure S7** Schematic digraph of a spheroid in a microwell. (a) Projection view and (b) Top view. Two zones can be divided in the microwell area, one is the spheroid area and another is the spheroid-free area. The impedance of a microwell containing a spheroid can be estimated according to method 2 in SI. Electric field lines simulated with COMSOL Multiphysics and a 2D model. The finite element analysis is applied to the microwells with and without tumor spheroid. For comparison, two types of microwell profiles were considered, microwells with a quasi-flat bottom (c) and microwells with a strong concave bottom (d). Without a tumor, the electric field is stronger inside the microwell than outside. In the presence of spheroids, the distribution of the field lines was perturbed. When the size of the spheroid is comparable to the size of the microwell, the electric field is highly condensed in the spheroid-free region, proving the critical spheroid size dependence on the electric properties of the system. More details are discussed in method 3 in SI.

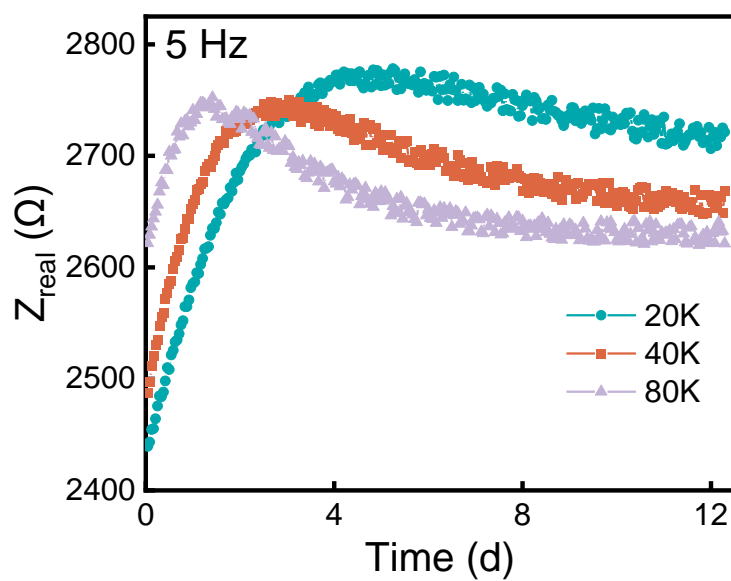


**Figure S8** Impedance spectra (real part) of the growing tumor spheroids in the PEGDA hydrogel microwells with different cell seeding numbers. The culture was performed with a microfluidic device for 12 days.

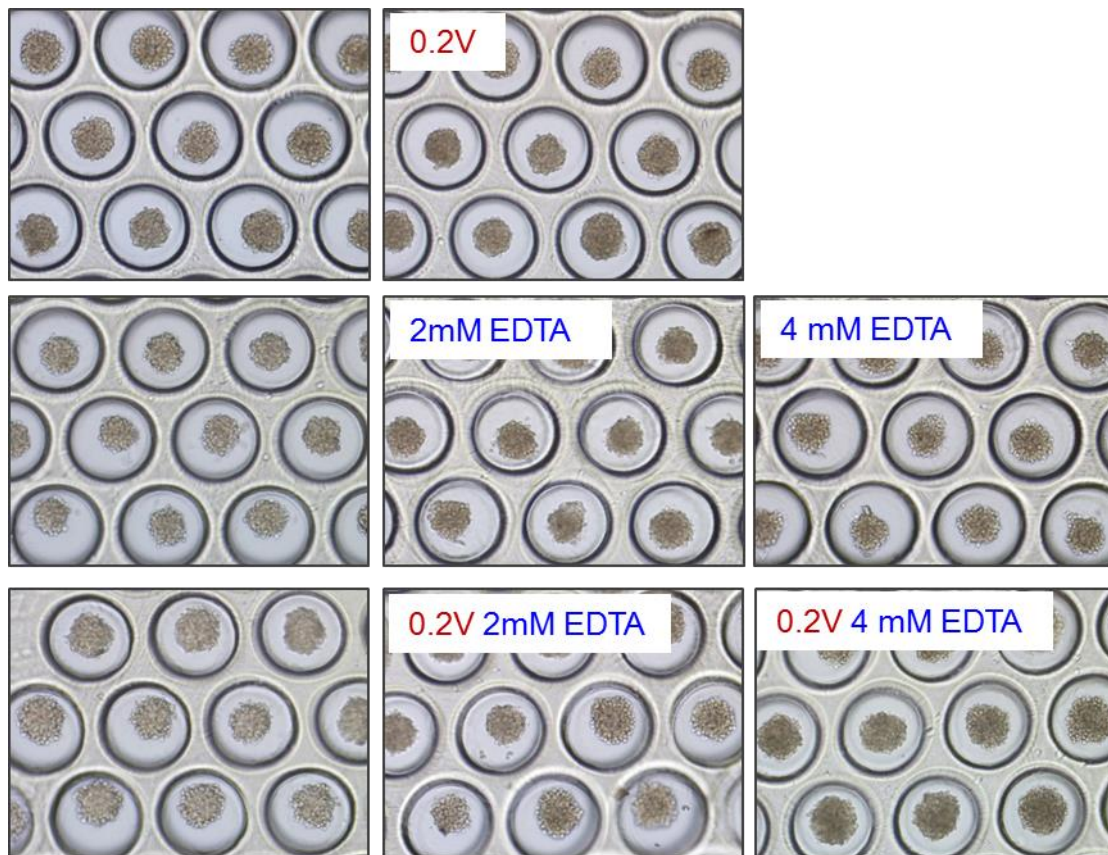


**Figure S9** Phase contrast images of tumor spheroids before and after biochemical (EDTA) and/or biophysical (0.2 V AC pulses) stimulation, Scale bar: 250  $\mu\text{m}$ .

## References

1. McMurtrey RJ. Analytic Models of Oxygen and Nutrient Diffusion, Metabolism Dynamics, and Architecture Optimization in Three-Dimensional Tissue Constructs with Applications and Insights in Cerebral Organoids. *Tissue Engineering Part C: Methods*. 2016;22:221–49.
2. Place TL, Domann FE, Case AJ. Limitations of oxygen delivery to cells in culture: An underappreciated problem in basic and translational research. *Free Radical Biology and Medicine*. 2017;113:311–22.
3. Zhadobov M, Augustine R, Sauleau R, Alekseev S, Di Paola A, Le Quément C, et al. Complex permittivity of representative biological solutions in the 2–67 GHz range. *Bioelectromagnetics*. 2012;33:346–55.
4. Carr L, Golzio M, Orlacchio R, Alberola G, Kolosnjaj-Tabi J, Leveque P, et al. A nanosecond pulsed electric field (nsPEF) can affect membrane permeabilization and cellular viability in a 3D spheroids tumor model. *Bioelectrochemistry*. 2021;141:107839.